NACA RM L50H08

NACA

RESEARCH MEMORANDUM

A TRANSONIC-WING INVESTIGATION IN THE LANGLEY 8-FOOT HIGH-SPEED TUNNEL AT HIGH SUBSONIC MACH NUMBERS AND AT A MACH NUMBER OF 1.2

WING-FUSELAGE CONFIGURATION WITH A WING OF 45° SWEEPBACK, ASPECT RATIO 4, TAPER RATIO 0.6, AND NACA 65A006 AIRFOIL SECTION

By Robert S. Osborne

Langley Aeronautical Laboratory
Langley Air Force Base, Va.

NATIONAL ADVISORY COMMITTEE
FOR AERONAUTICS

WASHINGTON

October 10, 1950

NACA RM L50H08

NATIONAL ADVISORY COMMITTEE FOR AERONAUTICS

RESEARCH MEMORANDUM

A TRANSONIC-WING INVESTIGATION IN THE LANGLEY 8-FOOT HIGH-SPEED TUNNEL AT HIGH SUBSONIC MACH NUMBERS AND AT A MACH NUMBER OF 1.2

WING-FUSELAGE CONFIGURATION WITH A WING OF 45° SWEEPBACK, ASPECT RATIO 4, TAPER RATIO 0.6, AND NACA 65A006 AIRFOIL SECTION

By Robert S. Osborne

SUMMARY

As part of an NACA research program, an investigation of a series of wing-fuselage configurations is being conducted in the Langley 8-foot high-speed tunnel to determine effects of wing geometry on aerodynamic characteristics. In the first part of this investigation, force, moment, wake, and downwash measurements were made on a fuselage and a wing-fuselage combination employing a wing with 45° sweepback of the 0.25-chord line, aspect ratio 4, taper ratio 0.6, and NACA 65A006 airfoil section parallel to the plane of symmetry at Mach numbers from 0.60 to 0.96 and at a Mach number of 1.2. The results are presented in this paper.

At low lift coefficients a decrease in lift-curve slope and a drag rise occurred for the wing-fuselage configuration at a Mach number of approximately 0.92, a rapid rearward movement of the aerodynamic center began at a Mach number of approximately 0.85, and a decrease in the rate of change of downwash angle with angle of attack began at a Mach number of approximately 0.90. With increases in lift coefficient above zero, the lift-curve slope increased and the aerodynamic center moved rearward at relatively low positive angles of attack. With further increases in angle of attack the lift-curve slope decreased and the aerodynamic center moved forward. In the region of the model base, flow disturbances due to the wake did not extend more than 0.25 semispan above the wing-chord plane for the conditions tested.

INTRODUCTION

As part of an NACA research program, a series of wing-fuselage configurations is being investigated in the Langley 8-foot high-speed tunnel to study the effects of wing geometry on the aerodynamic characteristics of wings at transonic speeds. In the first phase of the investigation, the effects of varying the sweepback of the 0.25-chord line of the wing are being determined.

The initial tests consisted of force, moment, wake, and downwash measurements on a fuselage and a wing-fuselage combination employing a wing with 45° sweepback of the 0.25-chord line, an aspect ratio of 4, a taper ratio of 0.6, and an NACA 65A006 airfoil section parallel to the plane of symmetry at Mach numbers from 0.60 to 0.96 and at a Mach number of 1.2. The results are presented in this paper.

The configurations used in these tests have been investigated in the Langley 7- by 10-foot tunnel utilizing the transonic-bump test technique, and a comparison of the results with those presented in this paper is presented in reference 1.

SYMBOLS

C_D	drag coefficient (D/qS)
C_L	lift coefficient (L/qS)
C_m	pitching-moment coefficient $\left(M_{\bar{c}/4}/qS\bar{c}\right)$
$\bar{c}$	wing mean aerodynamic chord, inches
D	drag, pounds
ΔH	loss of total pressure in wake, pounds per square foot
L	lift, pounds
M	Mach number
$M_{\bar{c}/4}$	pitching moment about $0.25\bar{c}$, inch-pounds
P_b	base pressure coefficient $\left(\frac{p_b - p_o}{q}\right)$
p_o	free-stream static pressure, pounds per square foot

p_b	static pressure at model base, pounds per square foot
q	free-stream dynamic pressure, pounds per square foot $\left(\frac{1}{2}\rho V^2\right)$
R	Reynolds number based on $\bar{c}$
S	wing area, square feet
V	free-stream velocity, feet per second
α	angle of attack of fuselage center line, degrees
ϵ	downwash angle, degrees
ρ	free-stream density, slugs per cubic foot

APPARATUS AND METHODS

Tunnel

The tests were conducted in the Langley 8-foot high-speed tunnel, which is of the closed-throat, single-return type. A plaster liner in the tunnel formed the subsonic test section at the geometric minimum and extended downstream to form the supersonic test section. The Mach number was uniform in the subsonic test section and varied by a maximum of 0.02 from the design Mach number of 1.2 in the supersonic test section (reference 2).

Model

The model was a midwing configuration. The wing was constructed of 14ST aluminum alloy and had 45° sweepback of the 0.25-chord line, an aspect ratio of 4, a taper ratio of 0.6, and an NACA 65A006 airfoil section parallel to the model plane of symmetry. The steel fuselage was hollow and was designed by cutting off the rearward part of a body of revolution with a fineness ratio of 12 to form a body with a fineness ratio of 10. A photograph of the model is shown as figure 1. Dimensional details are given in figures 2 and 3.

Measurements of the incidence of each half of the wing with the fuselage angle of attack of 0° revealed small inaccuracies of construction. The right wing had an incidence of 0.15° and the left wing an incidence of 0.05°. These inaccuracies are small and no attempt has been made to correct the data for them.

Model-Support System

The model was attached to an enclosed strain-gage balance at its forward end only, there being no other points of contact. At its downstream end, the balance was attached to a support tube through a straight coupling. The support tube was fixed axially in the center of the tunnel by two sets of support struts projecting from the tunnel walls. Location of the model in either the subsonic or supersonic test sections was accomplished by sliding the support tube forward or rearward on the support strut bearings. Details of the model-support system and the model locations in the subsonic and supersonic test sections are shown in figures 4 and 5.

The forward, tapered portion of the support tube was hinged to the rear portion in such a manner that angle-of-attack changes could be accomplished by means of an electric motor driving an actuating screw located within the tube. This mechanism was controlled from outside the test section and therefore permitted angle changes with the tunnel operating.

Measurements

Lift, drag, and pitching moment were determined by means of a strain-gage balance located inside the fuselage. Consideration of the accuracy of the strain-gage measurements and the magnitude of the scatter of a number of check points indicated the accuracy of the lift, drag, and pitching-moment coefficients to be approximately within ±0.01, ±0.001, and ±0.005, respectively, through the Mach number range.

The wake characteristics were measured at seven equally spaced locations from 0.125 to 0.375 semispans above the wing-chord plane. The "point" downwash angles were measured at locations 0.125, 0.250, and 0.375 semispans above the wing-chord plane. Both wake and downwash measurements were obtained at spanwise positions 0.083 and 0.292 semispans from the model plane of symmetry by means of two calibrated combination yaw-head and total-pressure rakes located 1.225 semispans behind the 25-percent mean-aerodynamic-chord position. These rakes were mounted on supports attached to the conical part of the support tube so that their positions with respect to the base of the model remained fixed with changes in model angle of attack. The measured downwash angles were estimated to be accurate to within $\pm 0.2^{\circ}$. Details of rake dimensions and locations are shown in figure 6. The static pressure at the base of the model was determined from a static orifice located in the side of the sting support at the plane of the model base.

The angles of the model and the rakes relative to the air stream were measured by a calibrated optical system consisting of mirrors mounted on

the upper surfaces of the fuselage and the rake supports and a point source of light mounted outside the tunnel. To determine the angle, the optical device containing the point source was adjusted until the reflected ray from the mirror coincided with the incident ray. The angle of the instrument with respect to the vertical was then measured with a vernier inclinometer. The use of this device in conjunction with the remotely controlled angle-of-attack changing mechanism allowed desired model angles to be set within $\pm 0.1^\circ$ with the tunnel operating at any Mach number.

Test Conditions

The tests were conducted through a Mach number range from 0.60 to approximately 0.96 with the model in the subsonic test section and at a Mach number of 1.2 in the supersonic test section. The fuselage configuration was tested at angles of attack from -4° to 14° at all Mach numbers, and the wing-fuselage configuration was tested from -2° to 14° at subsonic Mach numbers and from -2° to 10° at a Mach number of 1.2. The variation with Mach number of approximate test Reynolds number based on the wing mean aerodynamic chord is presented in figure 7.

Configurations included the wing-fuselage combination with natural transition and with transition fixed at 10 percent of the chord on the upper and lower surfaces of the wing and at 12 percent of the fuselage length, and the fuselage alone with natural transition only. Transition was fixed by a $\frac{1}{8}$-inch-wide strip composed of No. 60 carborundum grains imbedded in clear shellac. Unless otherwise noted, the data presented herein are for natural transition only.

During subsonic testing, static pressures along the tunnel wall at the model location were observed to insure that no data were obtained with the tunnel choked. For the tests at a Mach number of 1.2, the position of the normal shock relative to the model was indicated by shadow images of the shock formed on the tunnel wall by a parallel-beam light source. It was observed that the shock moved forward to the vicinity of the base of the model at high angles of attack. Since the results of tests reported in reference 3 indicated that this phenomenon seriously altered the pitching moment and drag of the model, and since the wake and downwash measurements would also be affected, such data have not been presented herein. Observation of tunnel-wall static pressures at a Mach number of 1.2 indicated that, at all test angles of attack, the shock disturbance from the nose of the model was transmitted to the wall sufficiently far downstream of the nose to insure that its reflection did not affect the model or the wake rakes.

CORRECTIONS

Blockage and Boundary-Induced Upwash

Expressions for correcting Mach number and dynamic pressure for effects of model and wake blockage and the drag coefficient for the effect of the pressure gradient caused by the wake were obtained from reference 4. Because the blockage factors presently available are applicable only to unswept wings, the value for a swept wing had to be approximated. Since the ratio of wing span to tunnel diameter was small and the wing was highly swept, it was assumed that the blockage factor for the wing would be the same as that for a body of revolution of volume equal to the exposed volume of the wing and length equal to the exposed length of the wing measured parallel to the air stream. The corrections thus obtained were approximately 7 percent less than would have been obtained with the assumption that the wing was unswept. The effects of boundary-induced upwash on the angles of attack and downwash were calculated from expressions presented in references 5 and 6. The effects of compressibility were considered in all cases.

The magnitude of the correction to Mach number was appreciable at subsonic Mach numbers of 0.85 and above, reaching 1.5 percent at a Mach number of 0.96. The corrections to the angles of downwash were significant at all subsonic Mach numbers tested for lift coefficients of approximately 0.3 and above, the maximum being an increment of 0.2°. These corrections have been applied to all data presented herein. The other errors caused by blockage and boundary-induced upwash were negligible and no corrections have been applied.

Tares

Because the balance system was an internal one, no forces on the sting support were measured, and the only tare was the interference effect of the sting support on the model. No specific tests were made to evaluate the tares for the configurations presented herein; however, the results of investigations of similar models and sting supports at low angles of attack which were presented in references 7 and 8 indicate that, since the present configuration did not include a horizontal tail, the pitching moment and lift tares were probably negligible. The effects of the sting on the drag coefficient presented in reference 7, when interpolated for the present configuration which had a ratio of sting area at the model base to area of model base of 0.677, indicated that the interference reduced the drag coefficient approximately 0.003 at subsonic speeds and 0.002 at a Mach number of 1.2. These values apply to both the fuselage-alone and wing-fuselage configurations. Because of the uncertainty of these corrections, especially at high

angles of attack, they have not been applied to the data presented herein except for comparison of drag data at zero lift and in calculation of maximum lift-drag ratios.

The interference of the sting support also affected the base pressures and the downwash angles. Interpolation of data obtained in connection with the tests reported in reference 7 indicated that at low angles of attack, the presence of the sting increased the base-pressure coefficients of the present fuselage-alone and wing-fuselage configurations approximately 0.1 at all Mach numbers tested. Also, the downwash angles may have been decreased by increments up to approximately 1° at subsonic Mach numbers and 0.1° at a Mach number of 1.2. Due to differences in angle of attack, afterbody shape, and location of the measuring devices in the flow field, the corrections are probably unreliable quantitatively and therefore have not been applied.

Wing Elasticity

The bending of a swept wing introduces effective twist which changes the loading characteristics. In order to determine the bending effects for the wing used in this investigation, theoretical methods were employed which required knowledge of the stiffness properties of the airfoil sections perpendicular to the 40-percent-chord line and the location of the effective root in bending. These values were obtained from static bending tests which consisted of applying concentrated loads on the 40-percent-chord line of the wing at 92 percent of the semispan from the plane of symmetry. Bending was found to occur about axes perpendicular to the 40-percent-chord line beginning at 23.5 percent of the geometric semispan measured from the plane of symmetry along the 40-percent-chord line. The moment of inertia of the airfoil section perpendicular to the 40-percent-chord line about the chord of that airfoil section was found to be the product of the chord and the cube of the maximum thickness divided by 26.5, with a modulus of elasticity of 10,300,000 pounds per square inch.

The foregoing assumptions were used in conjunction with spanwise lift distributions from references 9 and 10 to calculate the effects of bending on the lift and pitching-moment coefficients of the wing at a Mach number of 0.80, where it was indicated that essentially subcritical conditions existed. The results are presented in figure 8 and indicate that the slope of the lift curve was decreased approximately 7 percent and the aerodynamic center was moved forward approximately 2 percent of the mean aerodynamic chord. These corrections have not been applied since the spanwise lift distributions at Mach numbers above the critical were unknown and the bending could not be calculated.

Total Pressure Loss

The values of total pressure as measured by the wake rakes at a Mach number of 1.2 have been corrected for the loss due to the presence of the bow wave.

RESULTS AND DISCUSSION

An index of the figures presenting the results is as follows:

	Figure
Force and moment characteristics:	
C_L, C_D, and C_m plotted against M for -	
Wing-fuselage	9
Fuselage	10
P_b plotted against M for -	
Wing-fuselage	11(a)
Fuselage	11(b)
α, C_D, and C_m plotted against C_L for -	
Wing-fuselage	12
Wing with wing-fuselage interference	13
Summary	14 to 17
Wake and downwash characteristics:	
Wake data for -	
Wing-fuselage	18
Fuselage	19
ϵ plotted against α for -	
Wing-fuselage	20
Wing with wing-fuselage interference	20
Fuselage	21
$\frac{\partial \epsilon}{\partial \alpha}$ plotted against M for -	
Wing-fuselage	22
Wing with wing-fuselage interference	22
Effect of fixing transition on ϵ for -	
Wing-fuselage	23

Unless otherwise noted the data presented in the figures have not been corrected for sting tares and were obtained for the model with natural transition. In order to facilitate presentation of the data, staggered scales have been used in many of the figures and care should be taken in selecting the zero axis for each curve.

Force and Moment Characteristics

The effects of compressibility on the force and moment characteristics of the wing-fuselage configuration are shown in figure 9. At low lift coefficients the changes in lift coefficient with increase in Mach number were small. The lift obtained at an angle of attack of 0° may have been caused by a combination of inadvertent wing incidence, favorable interference due to the incidence, and angularity of flow in the tunnel. The drag rise occurred at a Mach number of approximately 0.92. Increases in Mach number above 0.85 at positive lift coefficients generally resulted in rapid decreases in pitching-moment coefficient.

The results of fixing transition at 10 percent of the chord on the upper and lower surfaces of the wing and at 12 percent of the fuselage length are also shown in figure 9. The effect on lift was negligible. At angles of attack from -2° to 6° the drag coefficients appeared to be increased by increments of 0.001 to 0.003 due to an increase in skin friction. At higher angles of attack no significant effect was noted. The effect on the pitching-moment coefficient was negligible except at a Mach number of 1.2 where at positive angles of attack the center of pressure appeared to be moved forward slightly.

The effects of compressibility on the lift and pitching-moment coefficients of the fuselage configuration (fig. 10) were negligible. A drag rise was indicated to occur in the untested Mach number range between 0.96 and 1.2.

The base pressure coefficients for the configurations tested are presented in figure 11. In general, fixing transition decreased the base pressures, and addition of the wing to the fuselage increased the values at high angles of attack.

The force and moment data for the wing-fuselage configuration are presented as a function of lift coefficient in figure 12. Similar data for the wing with wing-fuselage interference, obtained by a subtraction of fuselage values from wing-fuselage values, are presented in figure 13. The summary of these data is presented in figures 14 to 17.

At zero lift the lift-curve slope of the wing-fuselage configuration (fig. 14) increased from 0.057 at a Mach number of 0.60 to 0.076 at a Mach number of approximately 0.92. At a Mach number of 1.2 the value had decreased approximately to those observed at the lower subsonic speeds. At a lift coefficient of 0.4 the variation of lift-curve slope with Mach number was similar to that at zero lift, with the values being from 8 to 18 percent greater. This increase may have been due to an effectively increased camber of the airfoil caused by the separation bubble which is believed to form at relatively low angles of attack along the leading edges of the upper surfaces of sweptback wings having small leading-edge radii.

Low-speed tests of a similar wing conducted at various Reynolds numbers (reference 11) indicate that this phenomenon is influenced to a large extent by Reynolds number and is eliminated as the Reynolds number approaches a value of approximately 10×10^6. At higher angles of attack complete separation takes place over the wing tips and the lift-curve slopes decrease. As shown in figure 12(a), this separation is evident for the present wing at an angle of attack of approximately 10°.

The values of drag coefficient at zero lift for the wing-fuselage configuration were corrected for the tare due to sting interference as described previously and are compared with data from a rocket model of a similar configuration (reference 12) in figure 15. Agreement between the respective drag-rise Mach numbers and the values of drag coefficient was good.

The values of maximum lift-drag ratio presented in figure 16 decreased rapidly as the drag-rise Mach number of approximately 0.92 was reached. The values for the wing-fuselage configuration were calculated from drag coefficients which had been corrected for the tare due to sting interference. The uncertainty in the values of lift-drag ratio as a result of the inaccuracies in the lift and drag measurements for the wing-fuselage configuration was estimated to range from ±8 percent at a Mach number of 0.6 to ±4 percent at a Mach number of 1.2, and for the wing with wing-fuselage interference to vary from ±21 percent at a Mach number of 0.6 to ±7 percent at a Mach number of 1.2.

At zero lift the aerodynamic center of the wing-fuselage configuration (fig. 17) was at approximately 17 percent of the mean aerodynamic chord at a Mach number of 0.6. After a gradual rearward movement the aerodynamic center moved rapidly rearward with increases in Mach number above 0.85 to reach 33 percent of the mean aerodynamic chord at a Mach number of 0.96, and 38 percent at 1.2. At a lift coefficient of 0.4 the aerodynamic-center variation with Mach number was similar to that for the zero-lift case, with the aerodynamic center having moved approximately 7 percent farther rearward. This result may have been caused by a small rearward movement of the center of pressure resulting from the leading-edge separation previously mentioned. This separation decreases the magnitude of the leading-edge pressure peak and increases the chordwise extent of decreased pressure. At lift coefficients above 0.6 (fig. 12(c)), a forward destabilizing movement of the aerodynamic center occurred. This movement can be attributed to an inboard, forward shift in the center of pressure resulting from complete separation of the flow over the wing tips. As shown in figure 17, subtraction of the fuselage data from the wing-fuselage data moved the aerodynamic center rearward approximately 7 percent of the mean aerodynamic chord, the variation with Mach number remaining similar to that for the wing-fuselage configuration.

Wake and Downwash Characteristics

A representative selection of wake data for the wing-fuselage configuration presented in figure 18 for two spanwise positions indicated that, at a location 1.225 semispans behind the 25-percent point of the mean aerodynamic chord, the wake did not extend beyond a height approximately 0.25 semispan above the wing-chord plane for the angle and Mach number ranges of these tests. The increased intensity of the wake at the inboard location (fig. 18(b)) was probably due to the presence of the fuselage. This effect was shown by the wake data at the inboard location for the fuselage configuration. (See fig. 19.)

Downwash angles for the wing-fuselage configuration and the wing with wing-fuselage interference for two spanwise locations at three distances above the wing-chord plane are presented in figure 20. The data for the latter condition were obtained by subtraction of fuselage values from wing-fuselage values. It was indicated that the flow at the inboard location nearest the wing-chord plane was affected by the presence of the fuselage. This effect was further shown by the downwash angles for the same location for the fuselage configuration which are presented in figure 21. An examination of wake data at the inboard (0.083 semispan) location for the fuselage configuration indicated that the disturbance may have been caused by the wake of the fuselage.

In the evaluation of the downwash angles it was assumed that the local static pressure was equal to free-stream static pressure. Since this assumption may not be valid in the wake, the values of downwash angle presented for locations which lie in the wake may be in error by as much as approximately $+0.3^\circ$. This error is in addition to the previously discussed measurement error of $\pm 0.2^\circ$. Some of the irregularities at a Mach number of 1.2 may have been due to the effect on the wake rake of shock waves from the base of the model.

The rates of change of downwash angle with angle of attack were averaged for the two spanwise locations at a height 0.25 semispan above the wing-chord plane and are presented in figure 22. The variations with Mach number for the two configurations at both lift coefficients were generally erratic, the only definite tendency being a rapid decrease in $\frac{\partial \epsilon}{\partial \alpha}$ from approximately 0.6 to 0.2 in the Mach number range from 0.90 to 1.2.

The effect of fixing transition on the wake and downwash characteristics of the wing-fuselage configuration was negligible except at a Mach number of 1.2 where the downwash angles were increased as shown in figure 23. This result was probably due either to a change in the flow-separation characteristics of the wing or a change in the shock pattern in the region of the base of the model.

It was evident from the wake-width and downwash data that a horizontal tail located at the base of the model should not be located between 0.125 and 0.25 semispan above the wing-chord plane. Also, it appeared that predictions of tail characteristics involving theoretical downwash or measured downwash behind a wing alone must include the effects of fuselage interference in order to be accurate.

CONCLUSIONS

The following may be concluded from tests of a fuselage and a wing-fuselage combination employing a wing with 45° sweepback of the 0.25-chord line, aspect ratio 4, taper ratio 0.6, and NACA 65A006 airfoil section parallel to the plane of symmetry at high subsonic Mach numbers and at a Mach number of 1.2.

1. The effects of compressibility on the wing-fuselage configuration at low lift coefficients included a decrease in lift-curve slope and an increase in drag coefficient beginning at a Mach number of approximately 0.92, a rapid rearward movement of the aerodynamic center beginning at a Mach number of approximately 0.85, and a decrease in the rate of change of downwash angle with angle of attack beginning at a Mach number of approximately 0.90.

2. With increases in lift coefficient above zero the lift-curve slope increased and the aerodynamic center moved rearward at relatively low positive angles of attack because of the possible formation of a separation bubble on the leading edge of the wing. At an angle of attack of approximately 10°, it was indicated that complete separation over the wing tips resulted in abrupt decreases in lift-curve slope and a forward, unstable movement of the aerodynamic center.

3. The wake characteristics indicated that a horizontal tail located at the base of the model should not be located between 0.125 and 0.25 semispan above the wing-chord plane. Also, the necessity of including the effects of fuselage interference in theoretical downwash calculations was indicated.

Langley Aeronautical Laboratory
National Advisory Committee for Aeronautics
Langley Air Force Base, Va.

REFERENCES

1. Donlan, Charles J., Meyers, Boyd C., II, and Mattson, Axel T.: A Comparison of the Aerodynamic Characteristics at Transonic Speeds of Four Wing-Fuselage Configurations as Determined from Different Test Techniques. NACA RM L50H02, 1950.

2. Ritchie, Virgil S., Wright, Ray H., and Tulin, Marshall P.: An 8-Foot Axisymmetrical Fixed Nozzle for Subsonic Mach Numbers up to 0.99 and for a Supersonic Mach Number of 1.2. NACA RM L50A03a, 1950.

3. Ritchie, Virgil S.: Effects of Certain Flow Nonuniformities on Lift, Drag, and Pitching Moment for a Transonic-Airplane Model Investigated at a Mach Number of 1.2 in a Nozzle of Circular Cross Section. NACA RM L9E20a, 1949.

4. Herriot, John G.: Blockage Corrections for Three-Dimensional-Flow Closed-Throat Wind Tunnels with Consideration of the Effect of Compressibility. NACA RM A7B28, 1947.

5. Eisenstadt, Bertram J.: Boundary-Induced Upwash for Yawed and Swept-Back Wings in Closed Circular Wind Tunnels. NACA TN 1265, 1947.

6. Goldstein, S., and Young, A. D.: The Linear Perturbation Theory of Compressible Flow with Application to Wind-Tunnel Interference. R. & M. No. 1909, British A.R.C., 1943.

7. Osborne, Robert S.: High-Speed Wind-Tunnel Investigation of the Longitudinal Stability and Control Characteristics of a $\frac{1}{16}$-Scale Model of the D-558-2 Research Airplane at High Subsonic Mach Numbers and at a Mach Number of 1.2. NACA RM L9C04, 1949.

8. Luoma, Arvo A., and Wright, John B.: Longitudinal Stability and Control Characteristics at High-Subsonic Speeds of Two Models of a Transonic Research Airplane with Wings and Horizontal Tails of Aspect Ratio 4.2 and 2. NACA RM L50H07, 1950.

9. DeYoung, John: Theoretical Additional Span Loading Characteristics of Wings with Arbitrary Sweep, Aspect Ratio, and Taper Ratio. NACA TN 1491, 1947.

10. Diederich, Franklin W.: A Simple Approximate Method for Obtaining Spanwise Lift Distributions over Swept Wings. NACA RM L7I07, 1947.

11. Cahill, Jones F., and Gottlieb, Stanley M.: Low-Speed Aerodynamic Characteristics of a Series of Swept Wings Having NACA 65A006 Airfoil Sections. NACA RM L9J20, 1949.

12. Katz, Ellis: Flight Investigation from High Subsonic to Supersonic Speeds to Determine the Zero-Lift Drag of a Transonic Research Vehicle Having Wings of 45° Sweepback, Aspect Ratio 4, Taper Ratio 0.6, and NACA 65A006 Airfoil Sections. NACA RM L9H30, 1949.



Figure 1.- Photograph of the model as tested in the Langley 8-foot high-speed tunnel.

Wing Details

Airfoil section (parallel to plane of symmetry)	NACA 65A006
Area, sq ft	1
Aspect ratio	4
Taper ratio	0.6
Incidence, deg	0
Dihedral, deg	0
Geometric twist, deg	0

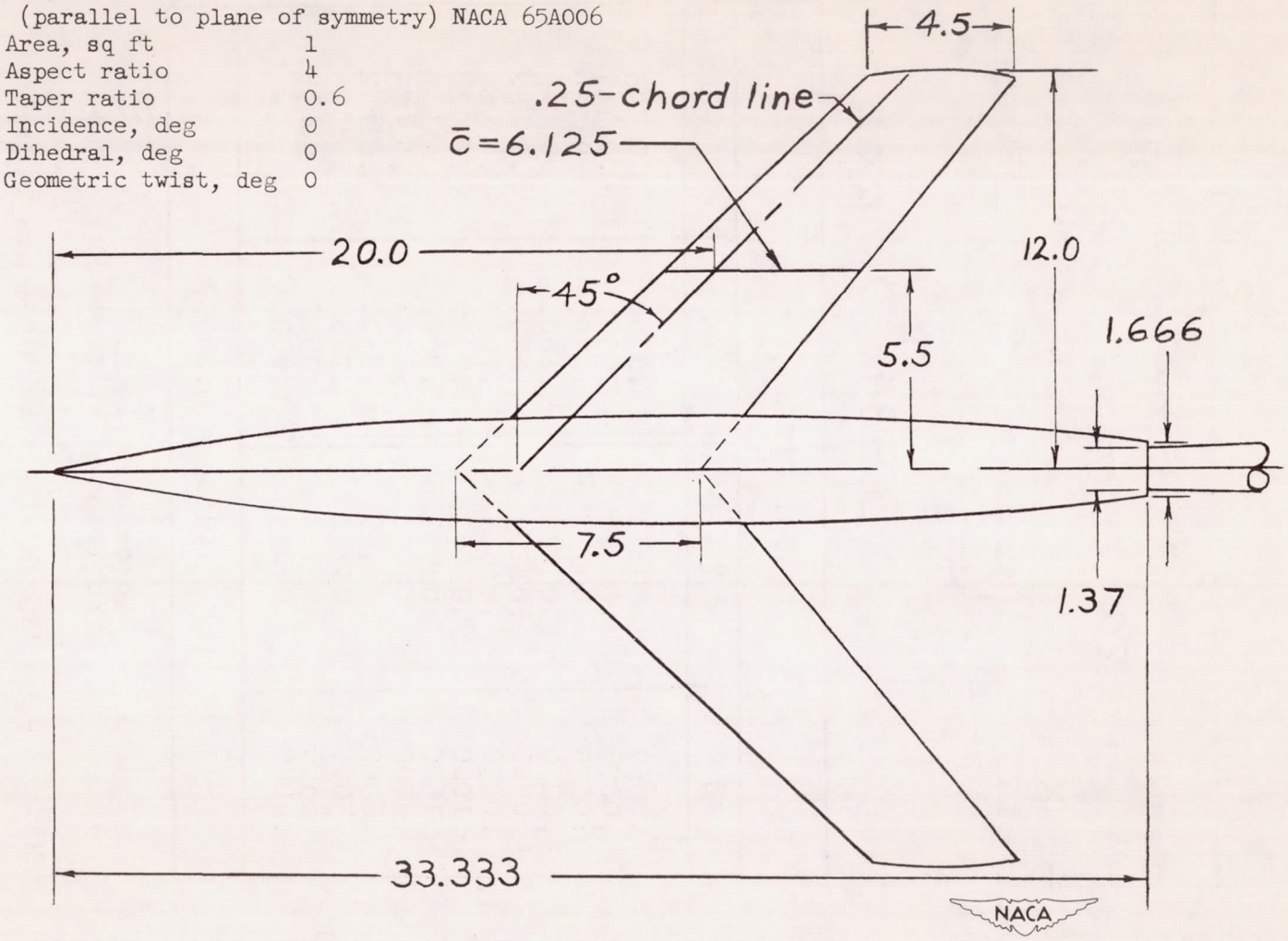
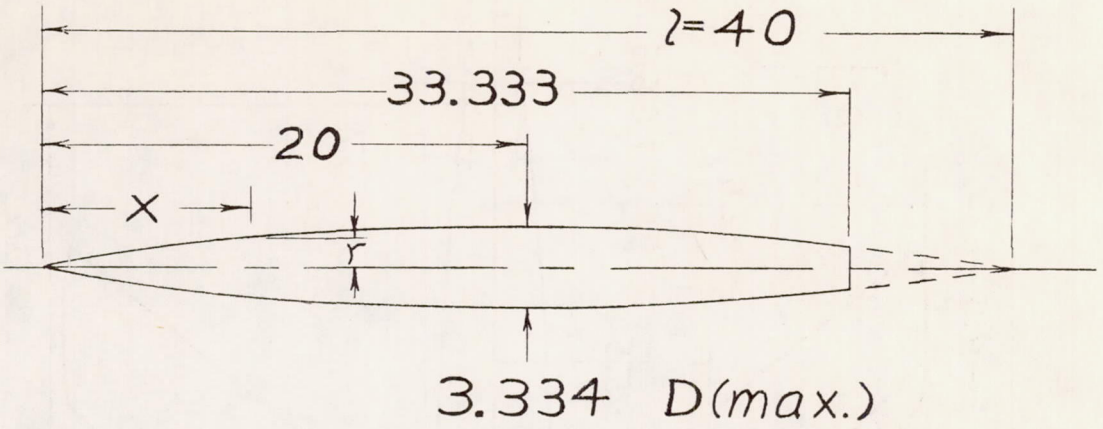


Figure 2 - Model details. All dimensions in inches.



ORDINATES			
x/l	r/l	x/l	r/l
0	0		
.0050	.00231	.4500	.04143
.0075	.00298	.5000	.04167
.0125	.00428	.5500	.04130
.0250	.00722	.6000	.04024
.0500	.01205	.6500	.03842
.0750	.01613	.7000	.03562
.1000	.01971	.7500	.03128
.1500	.02593	.8000	.02526
.2000	.03090	.8333	.02083
.2500	.03465	.8500	.01852
.3000	.03741	.9000	.01125
.3500	.03933	.9500	.00439
.4000	.04063	1.0000	0
L.E. radius = 0.0005l			

Fineness ratio 10
$\overline{c}/4$ located at D(max.)

Figure 3.- Fuselage details. All dimensions in inches.

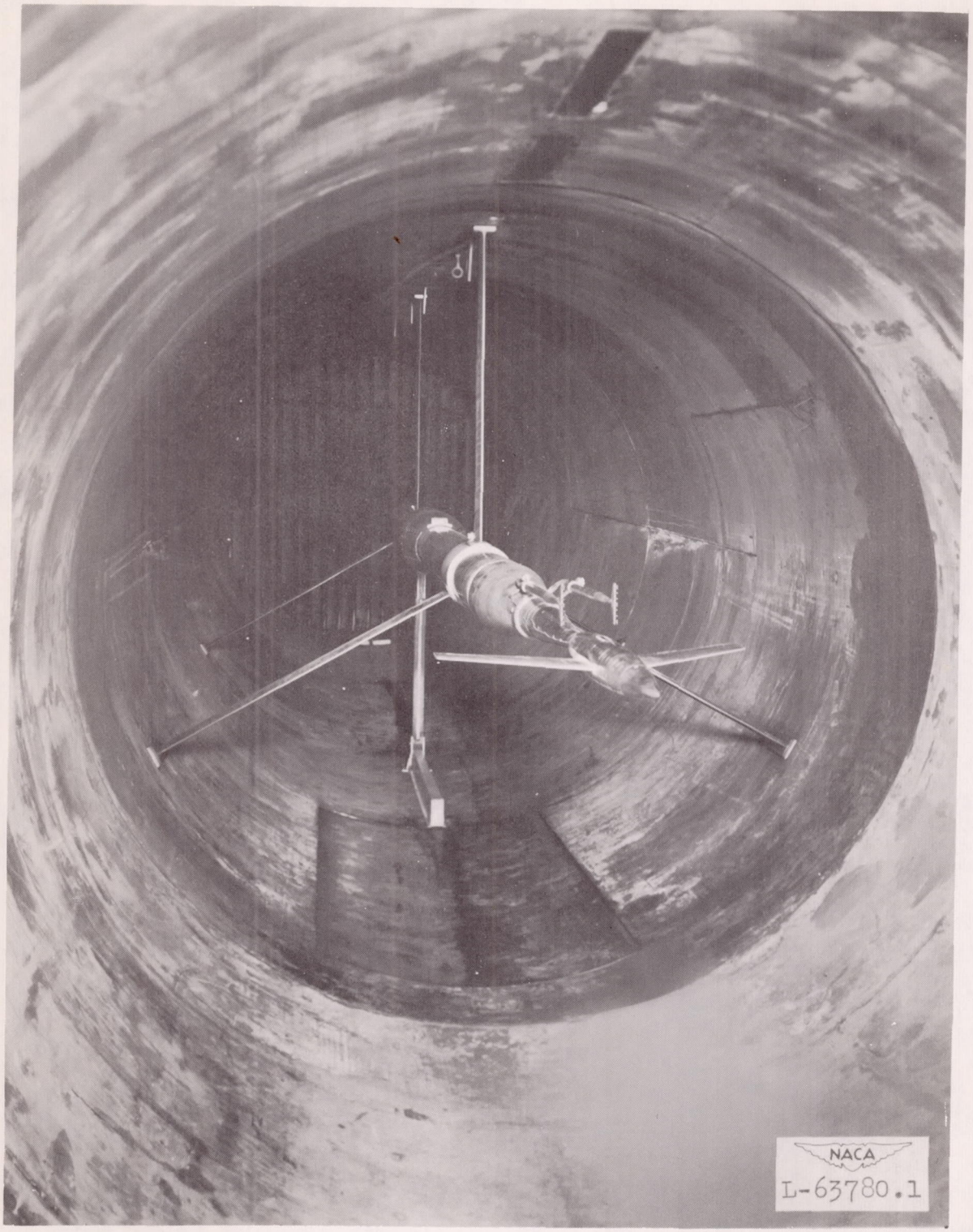


Figure 4.- Photograph of the model and the model support system, Langley 8-foot high-speed tunnel.

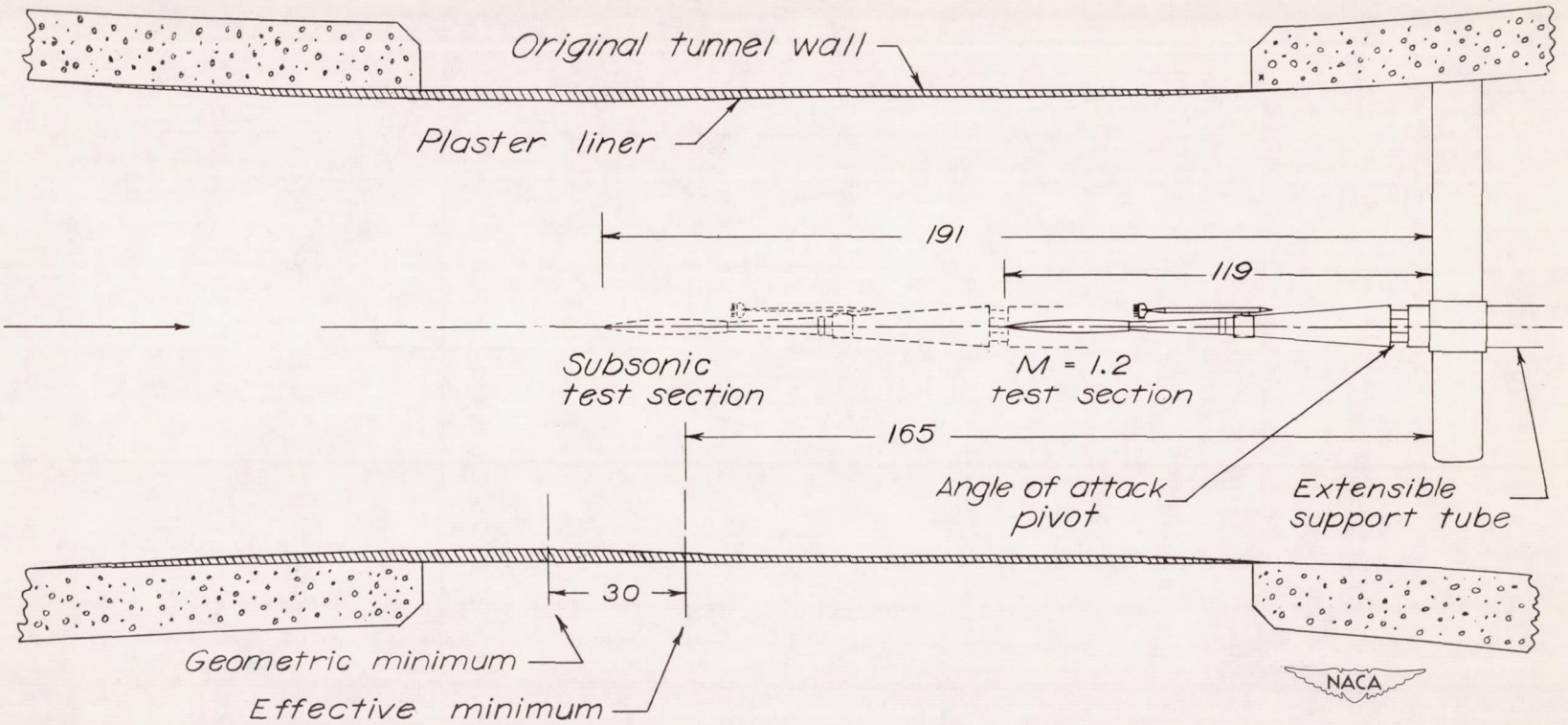


Figure 5.- Location of model in subsonic and supersonic test sections of Langley 8-foot high-speed tunnel. All dimensions in inches.

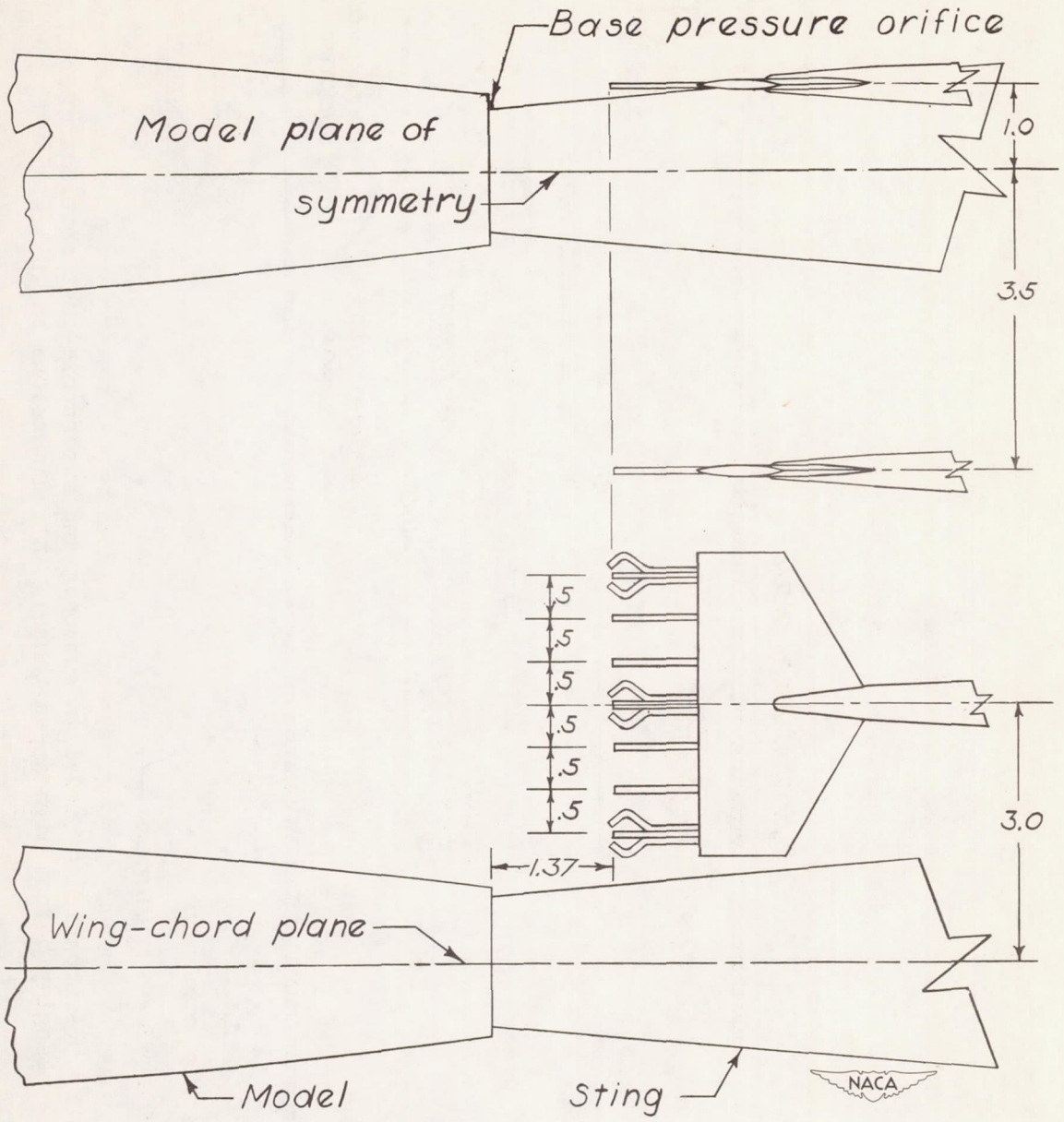


Figure 6.- Location and dimensions of the wake rakes. All dimensions in inches.

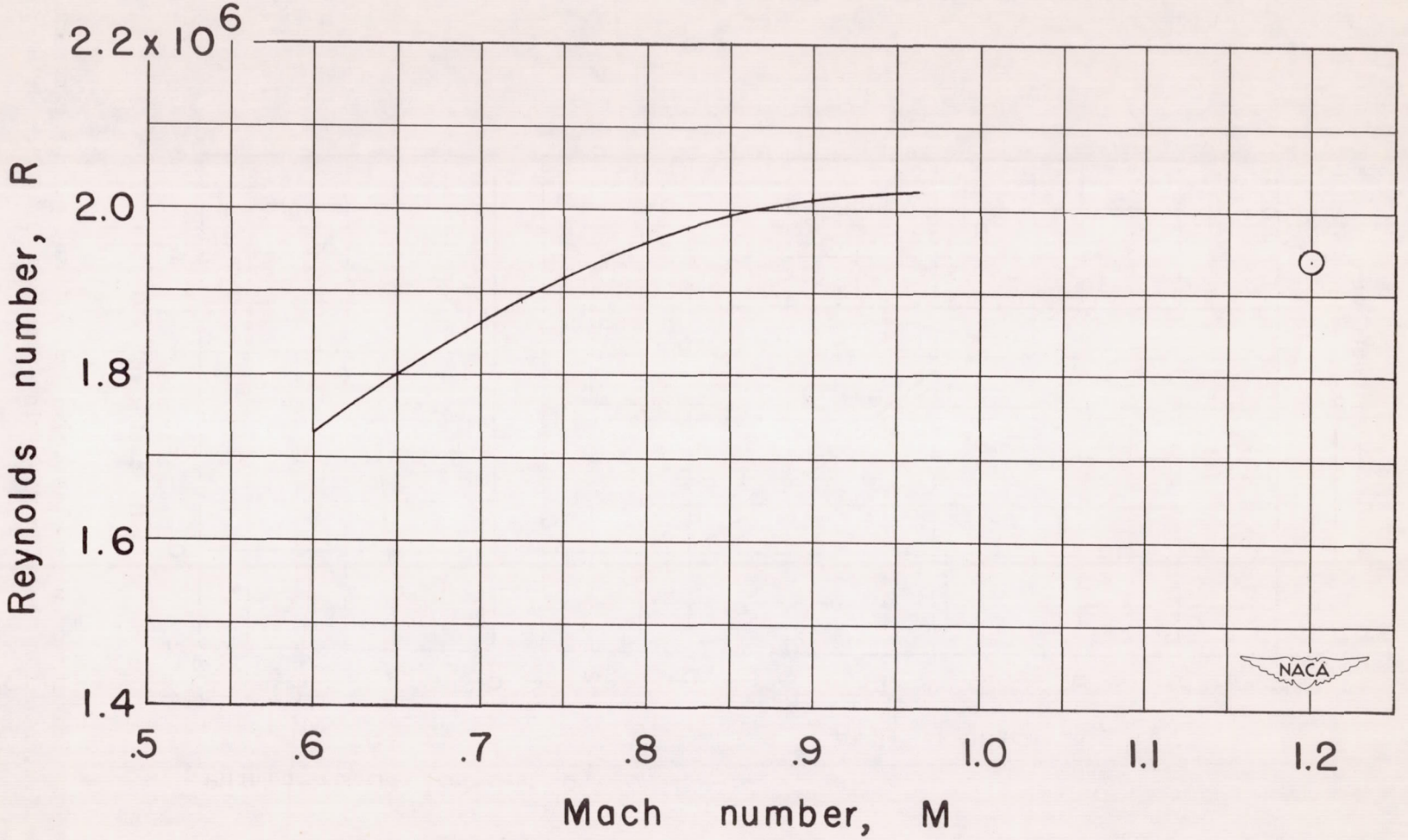


Figure 7.- Variation with Mach number of test Reynolds number based on a $\bar{c}$ of 6.125 inches.

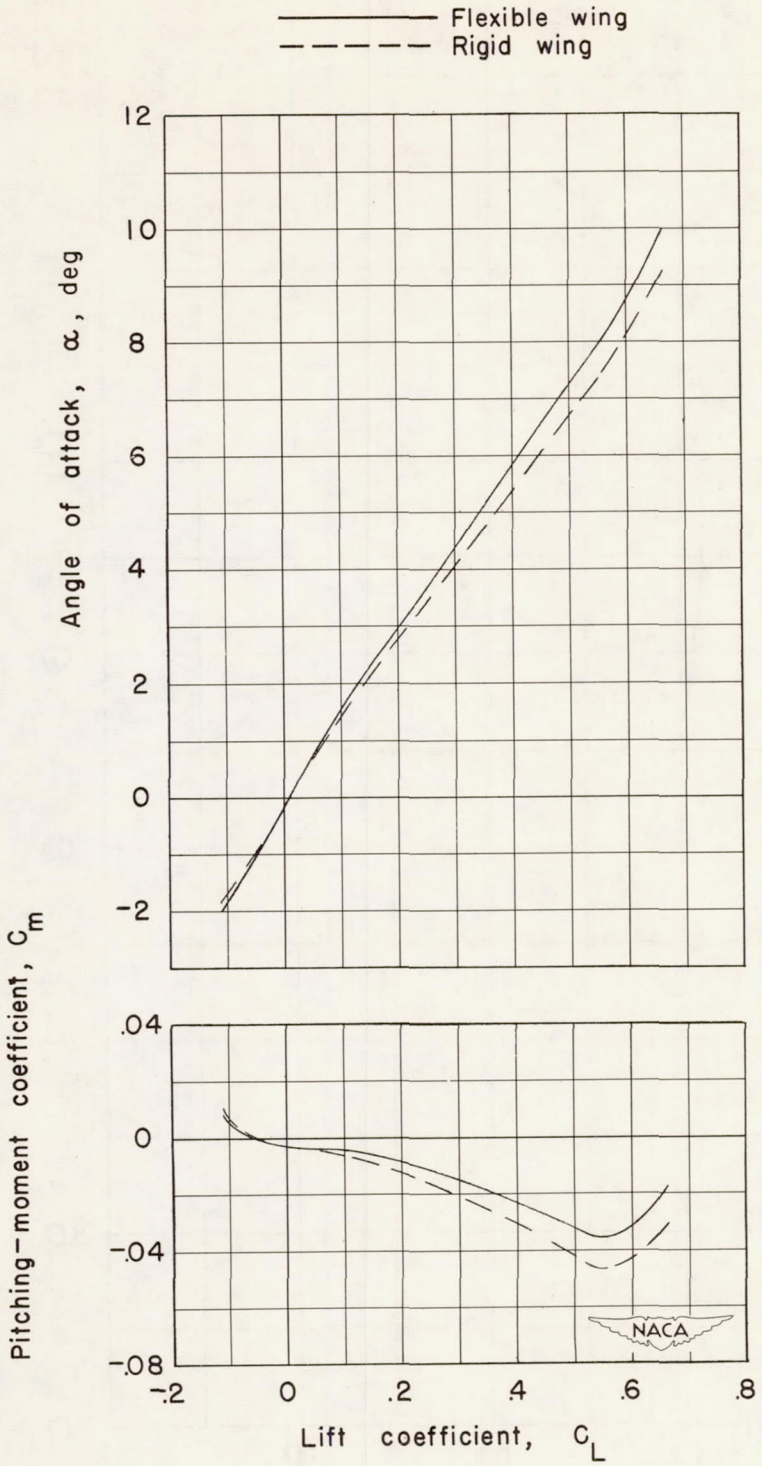
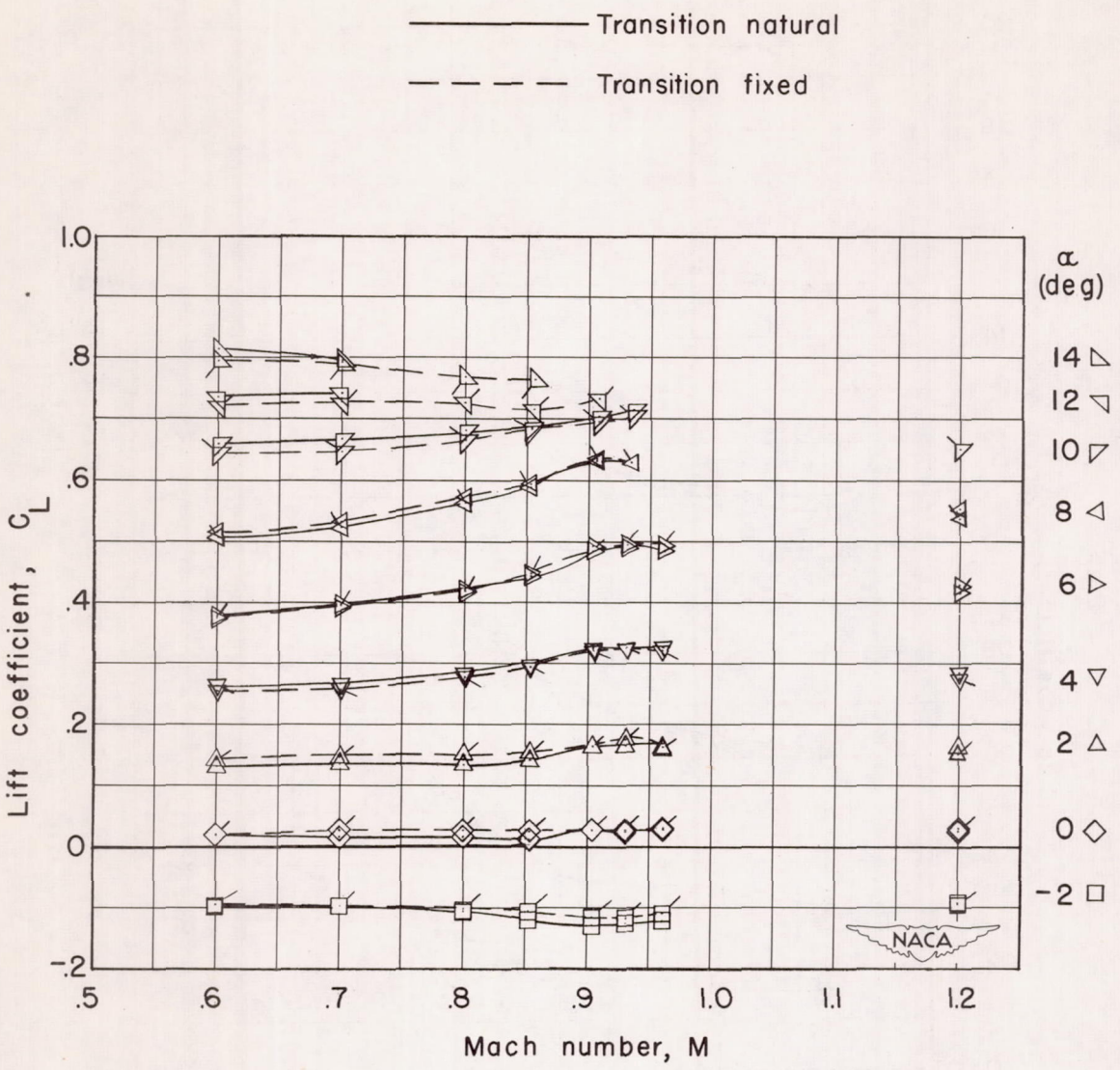
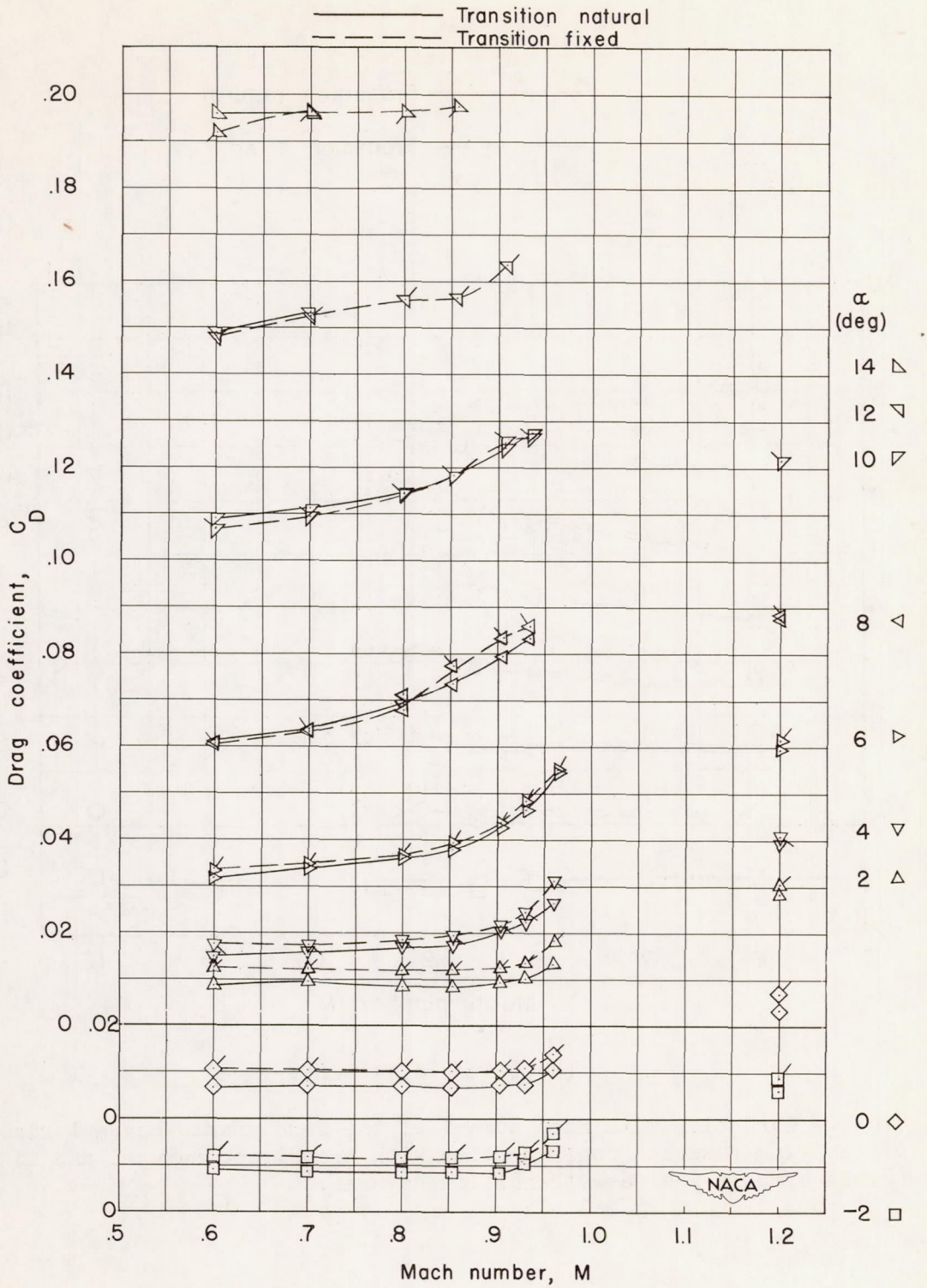


Figure 8.- Effects of wing elasticity on lift and pitching-moment coefficients for the wing with wing-fuselage interference at a Mach number of 0.80.



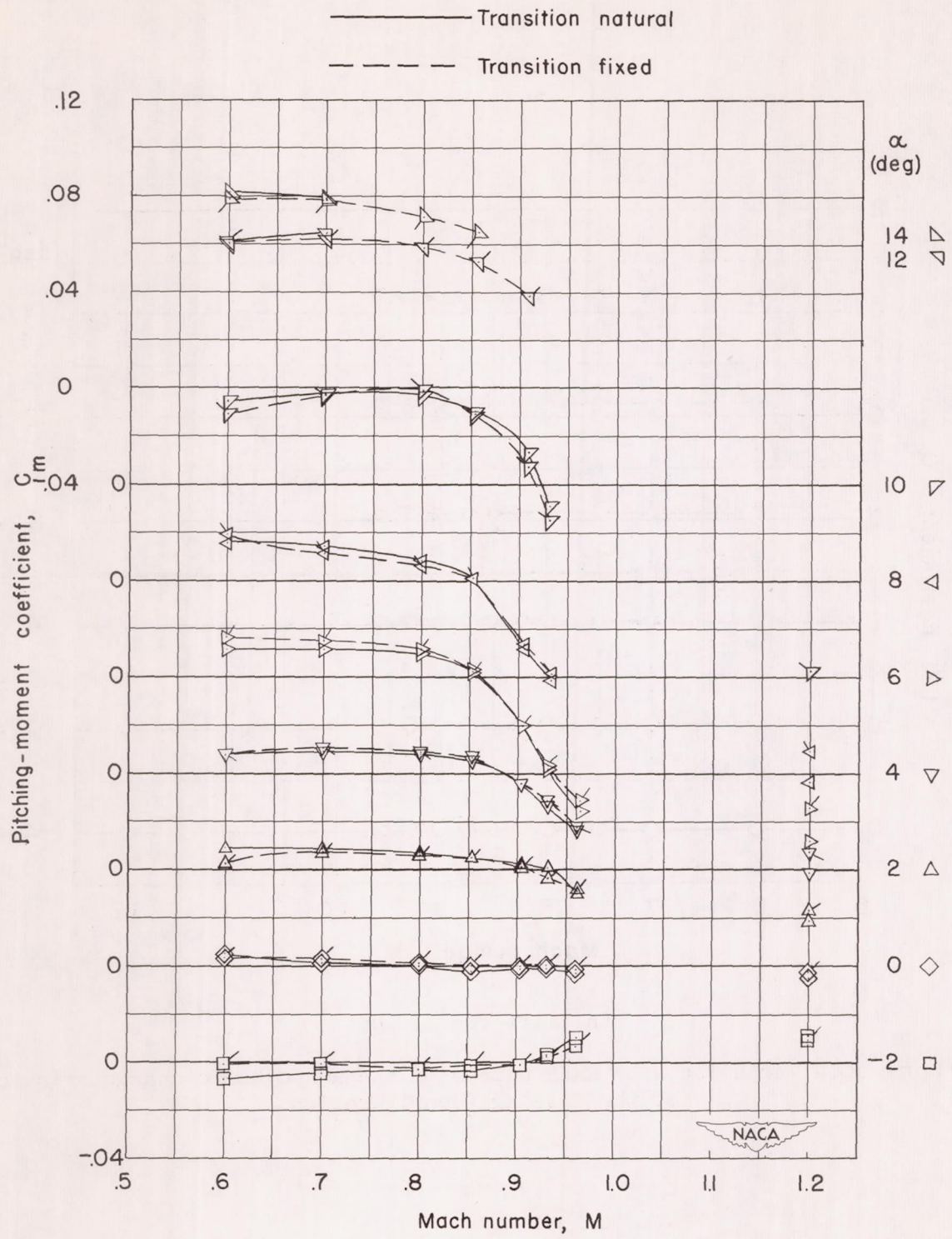
(a) Lift coefficient.

Figure 9.- Variation with Mach number of the aerodynamic characteristics of the wing-fuselage configuration with transition natural and fixed. (Plain symbols indicate transition natural.)



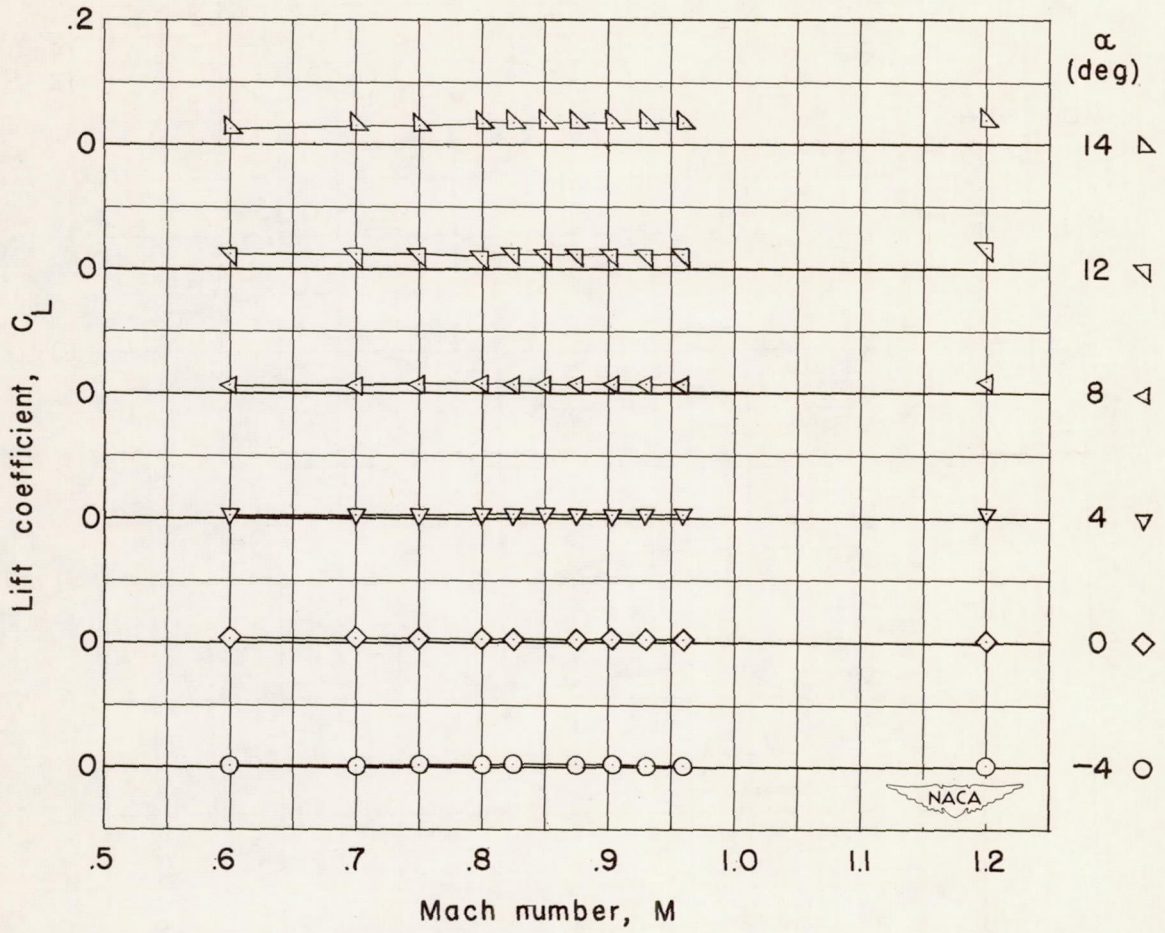
(b) Drag coefficient.

Figure 9.- Continued.



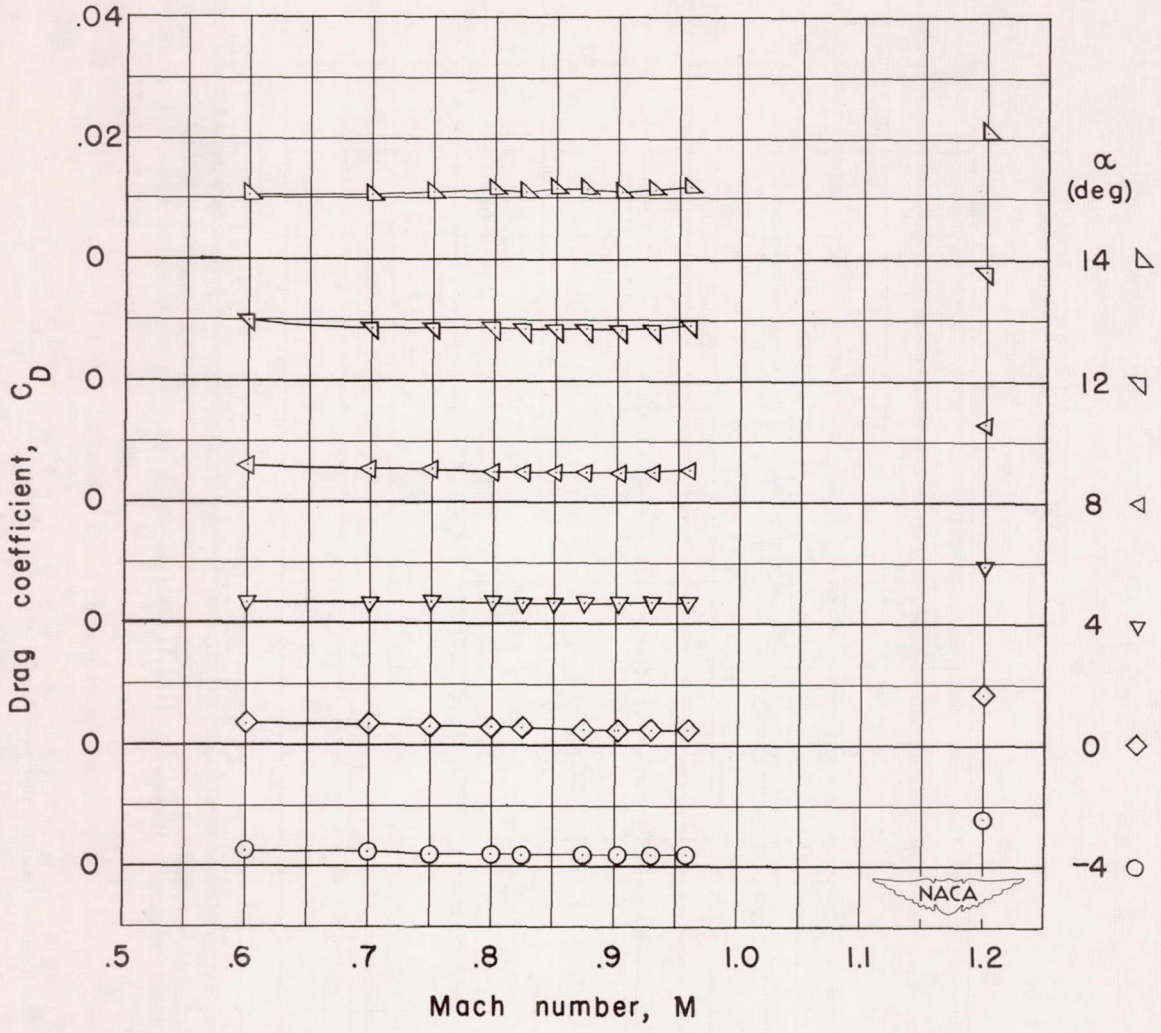
(c) Pitching-moment coefficient.

Figure 9.- Concluded.



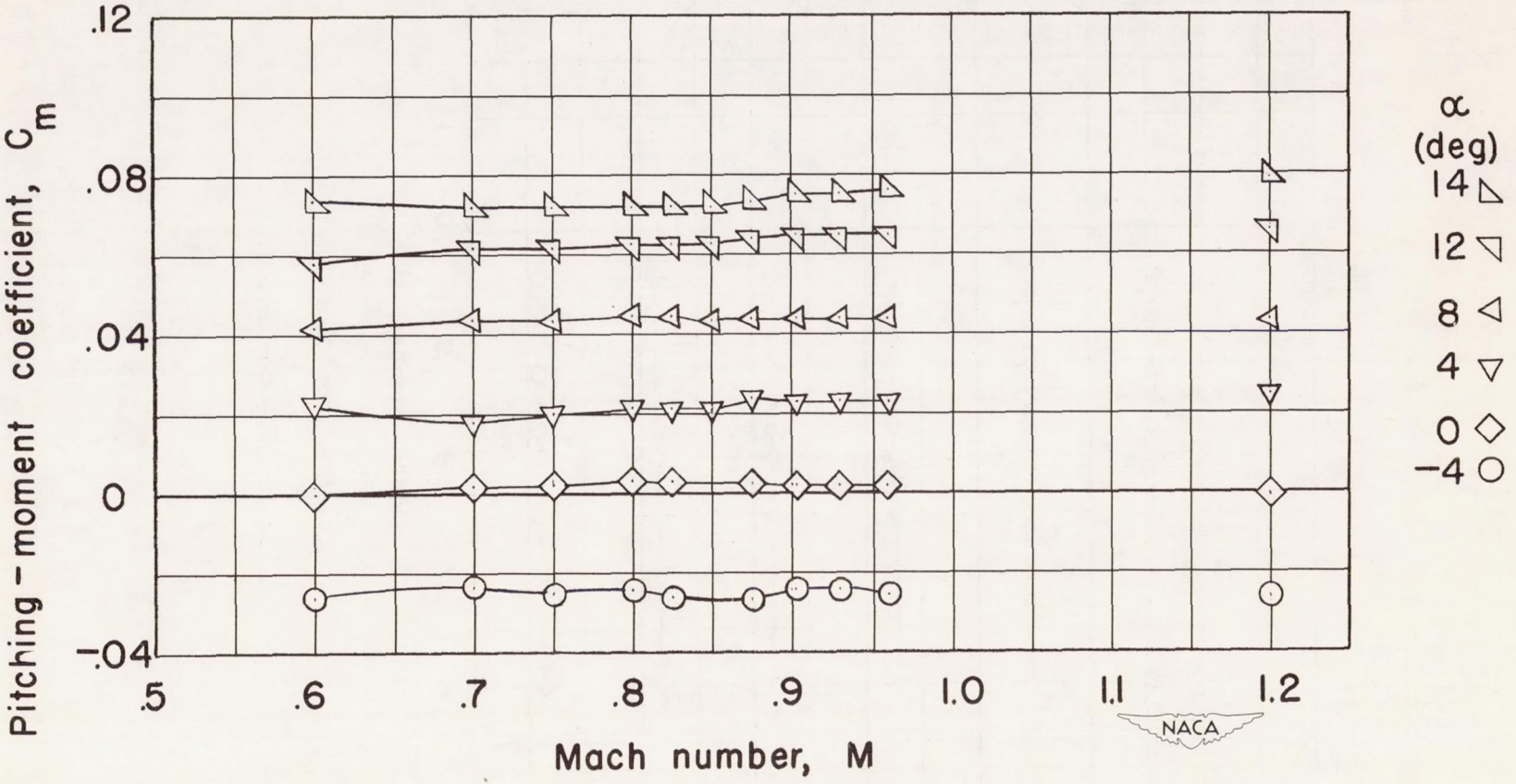
(a) Lift coefficient.

Figure 10.- Variation with Mach number of the aerodynamic characteristics of the fuselage configuration.



(b) Drag coefficient.

Figure 10.- Continued.



(c) Pitching-moment coefficient.

Figure 10.- Concluded.

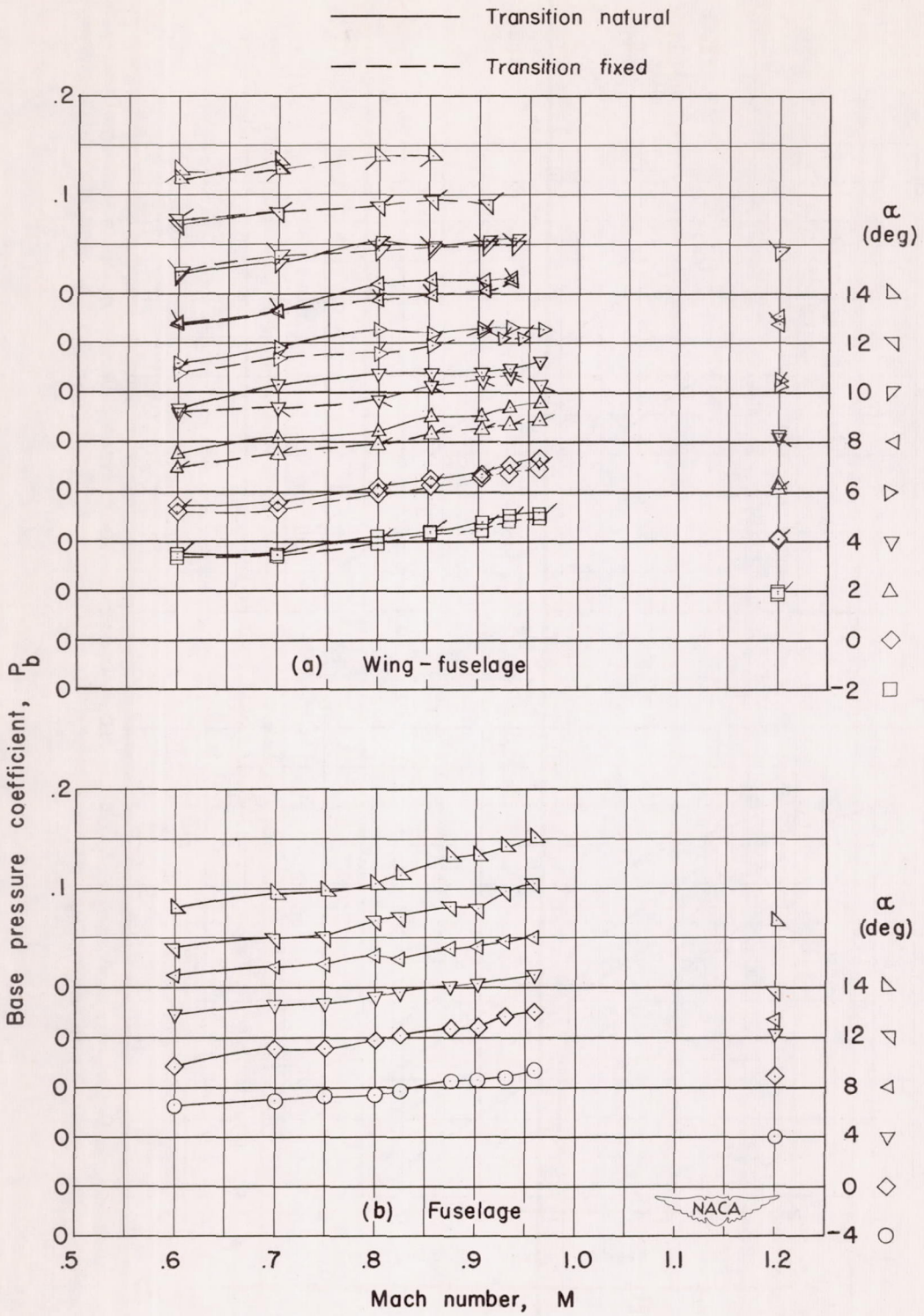
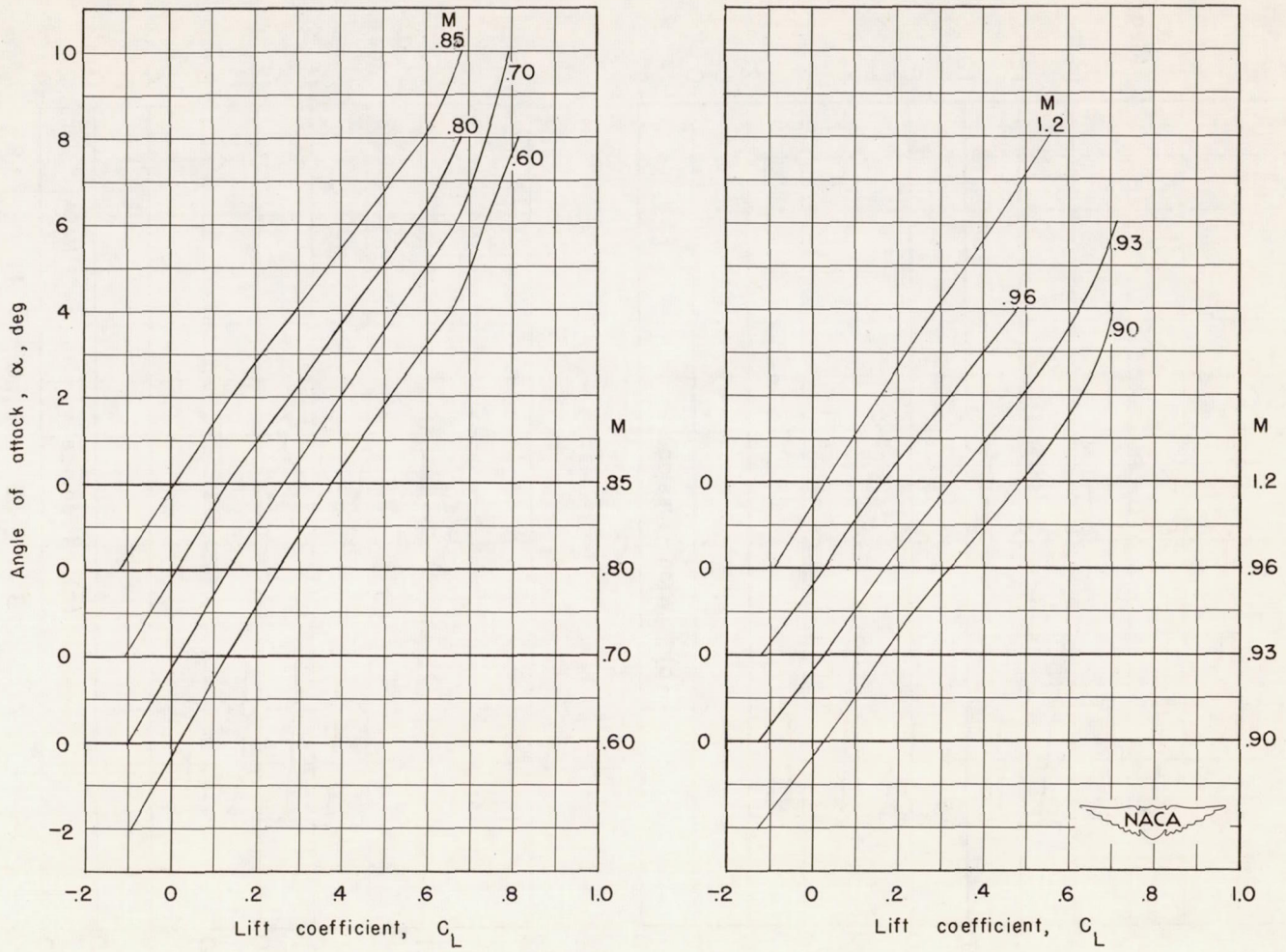
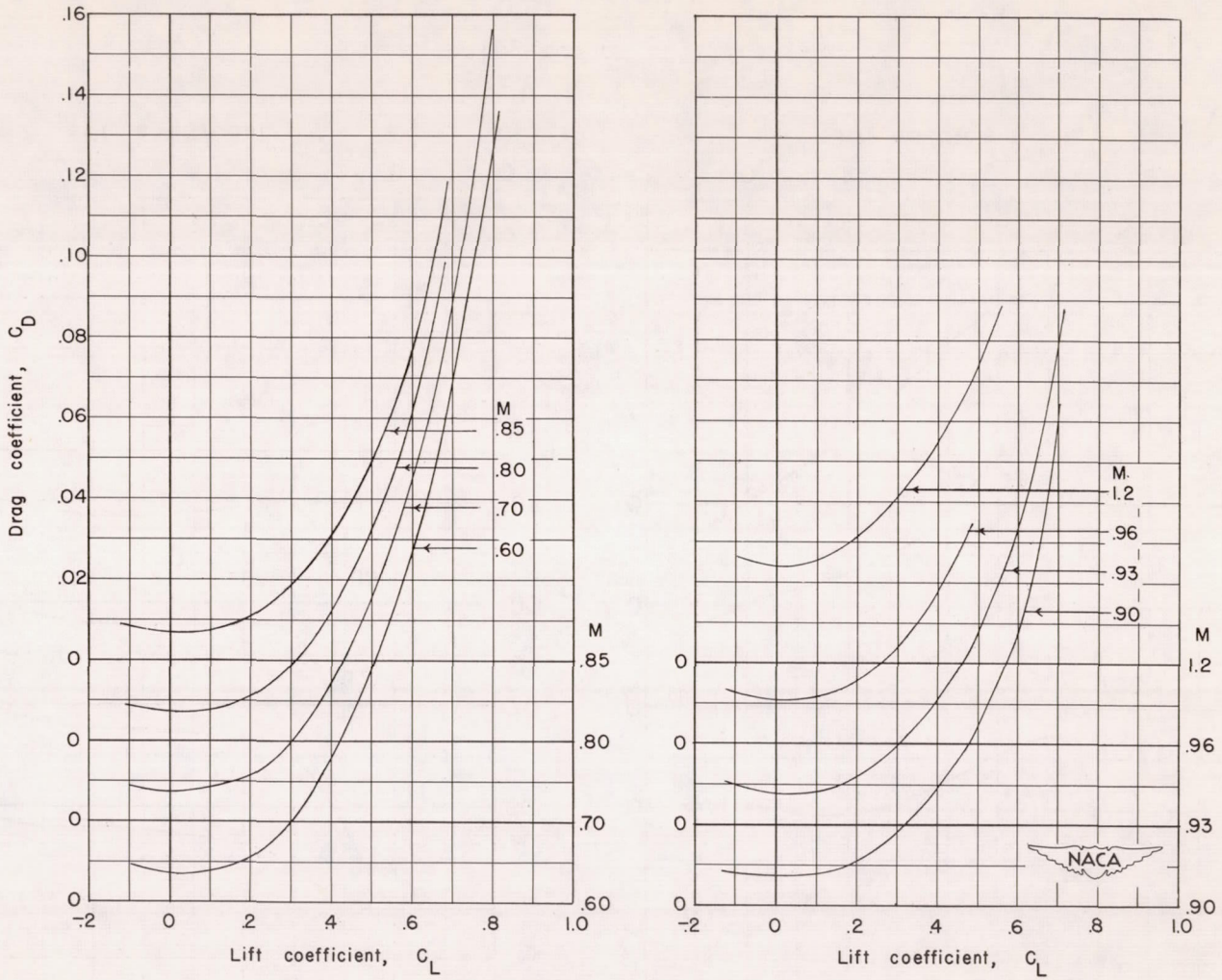


Figure 11.- Variation of base pressure coefficient with Mach number for the wing-fuselage and the fuselage configurations. (Plain symbols indicate transition natural.)



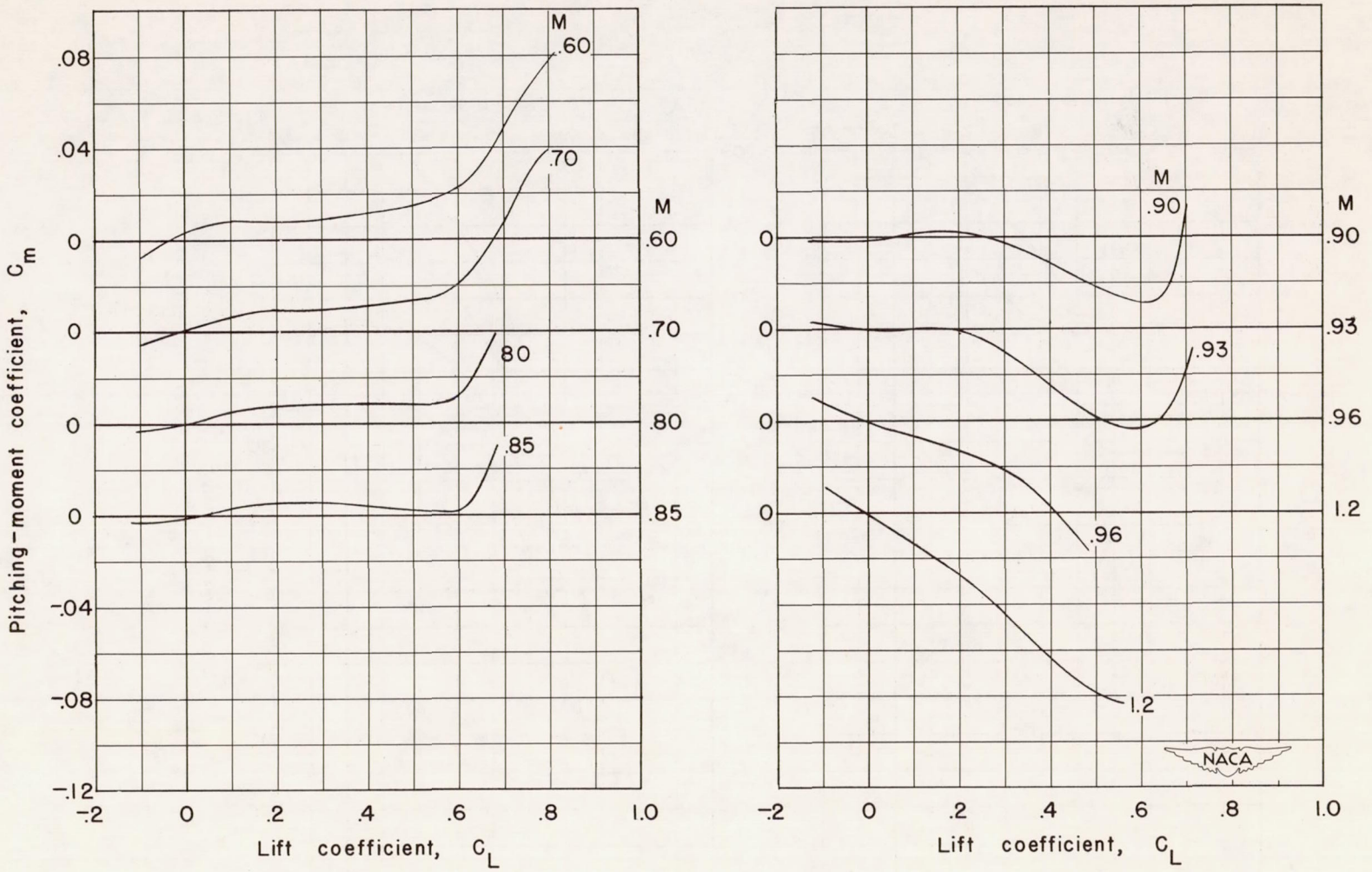
(a) Angle of attack.

Figure 12.- Variation with lift coefficient of the aerodynamic characteristics of the wing-fuselage configuration.



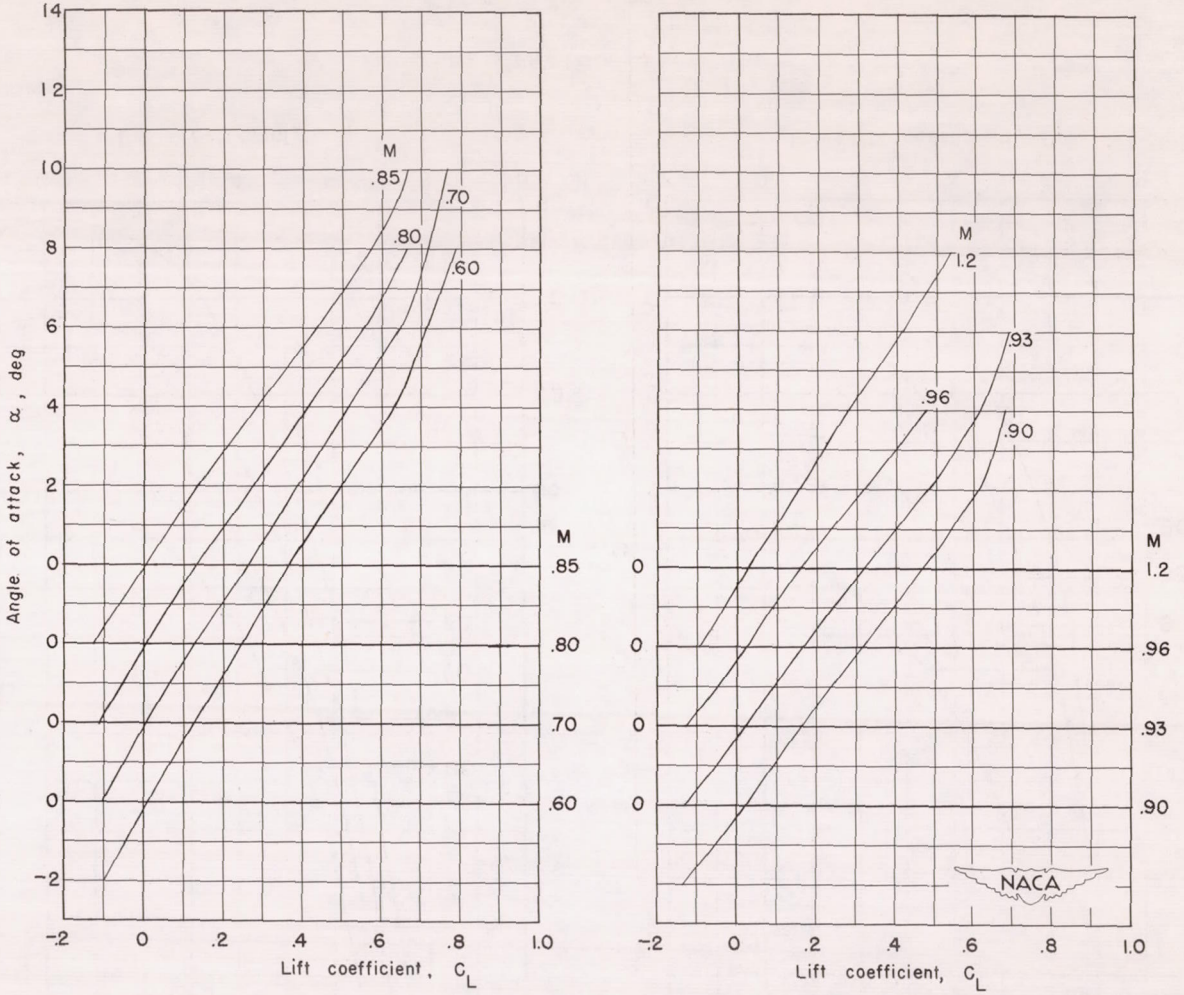
(b) Drag coefficient.

Figure 12.- Continued.



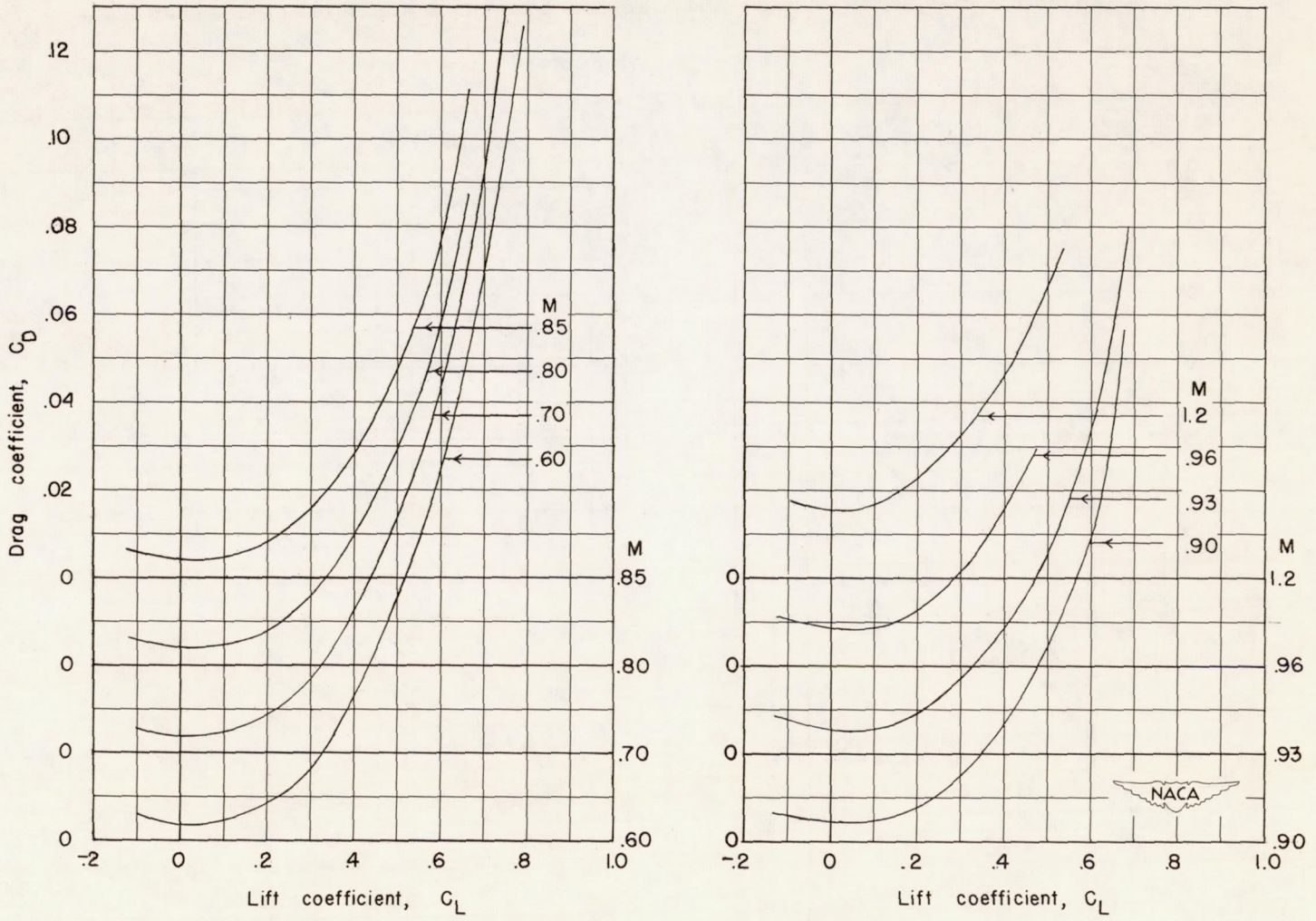
(c) Pitching-moment coefficient.

Figure 12.- Concluded.



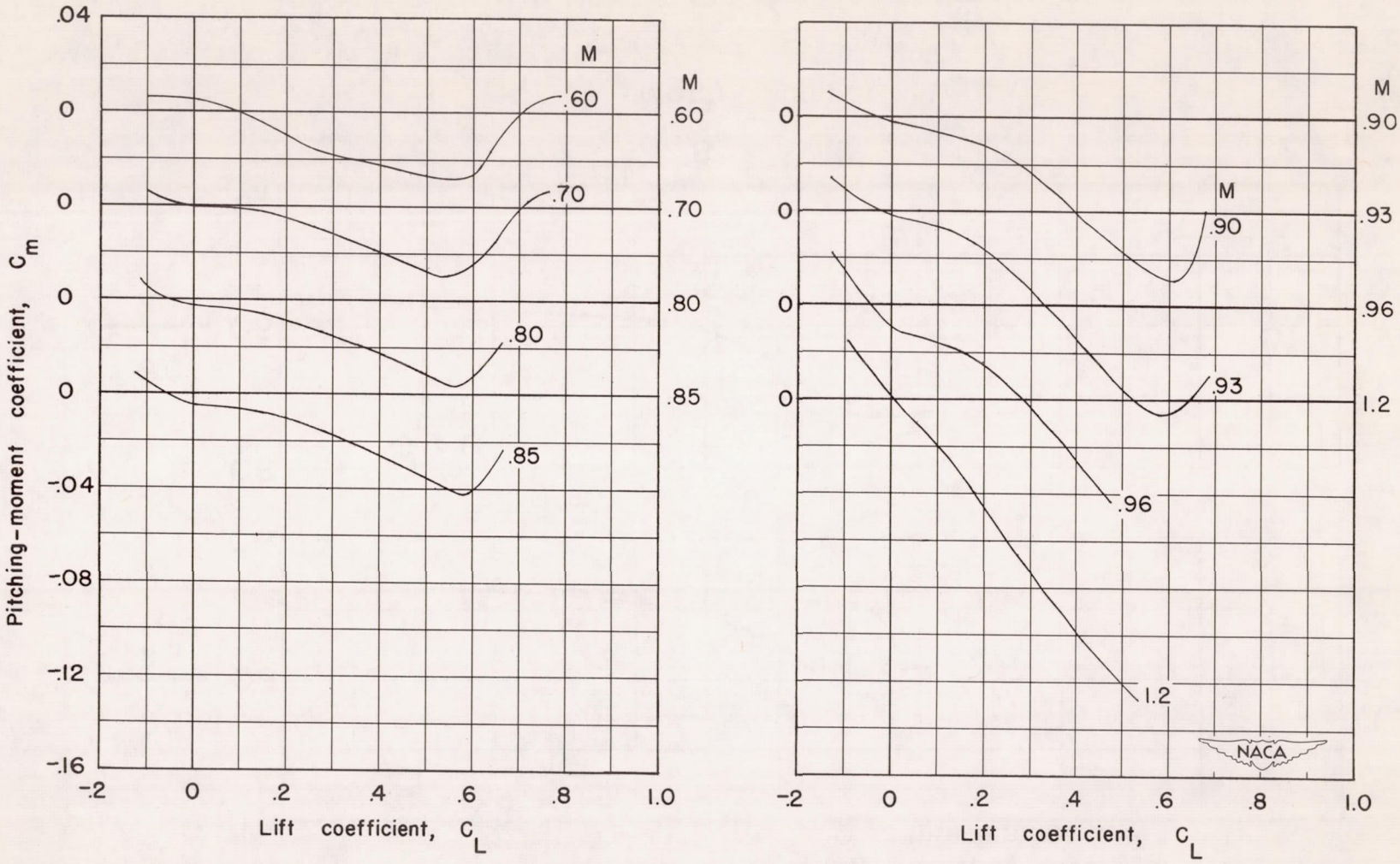
(a) Angle of attack.

Figure 13.- Variation with lift coefficient of the aerodynamic characteristics of the wing with wing-fuselage interference.



(b) Drag coefficient.

Figure 13.- Continued.



(c) Pitching-moment coefficient.

Figure 13.- Concluded.

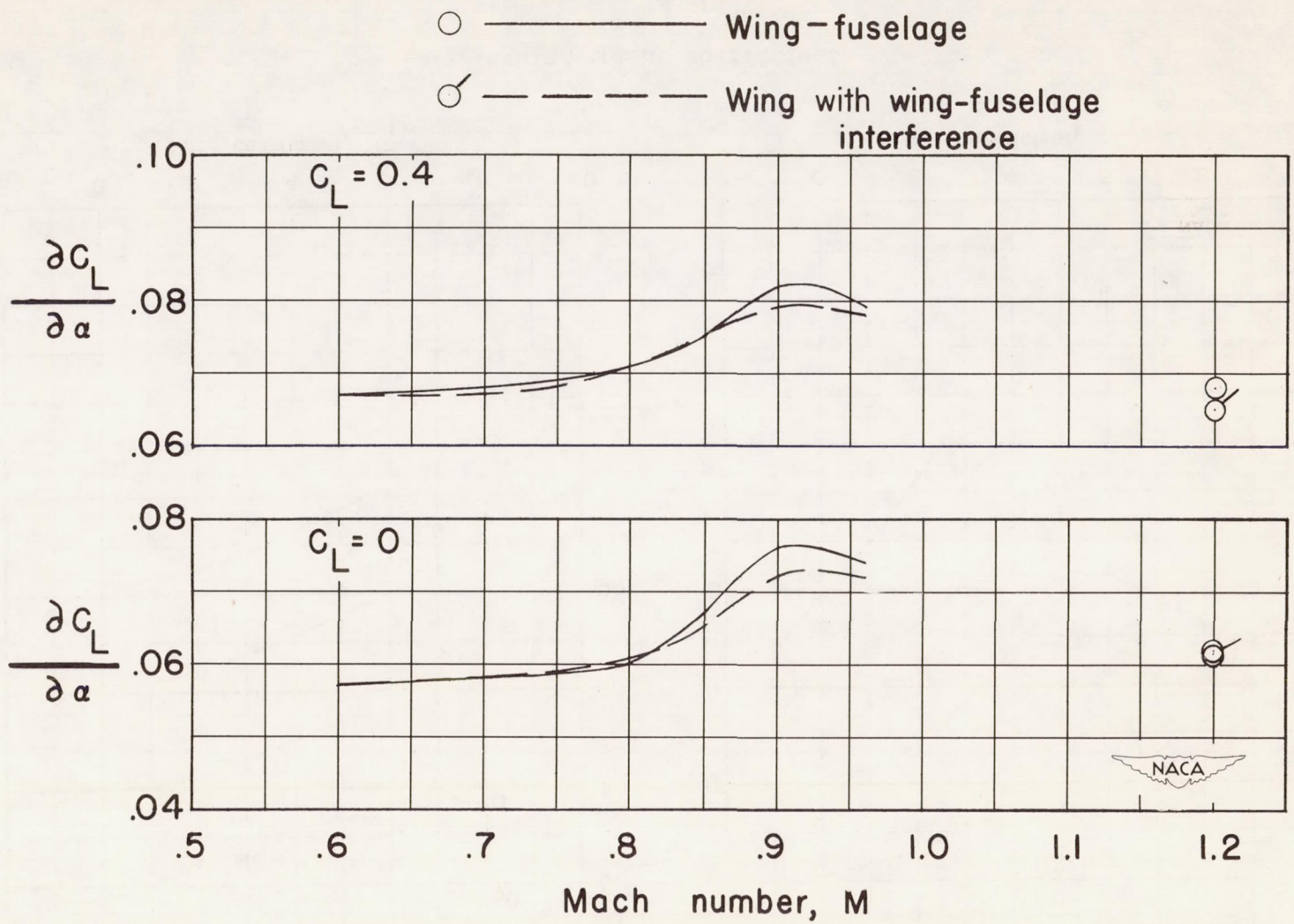


Figure 14.- Variation of lift-curve slope with Mach number for the wing-fuselage configuration and the wing with wing-fuselage interference.

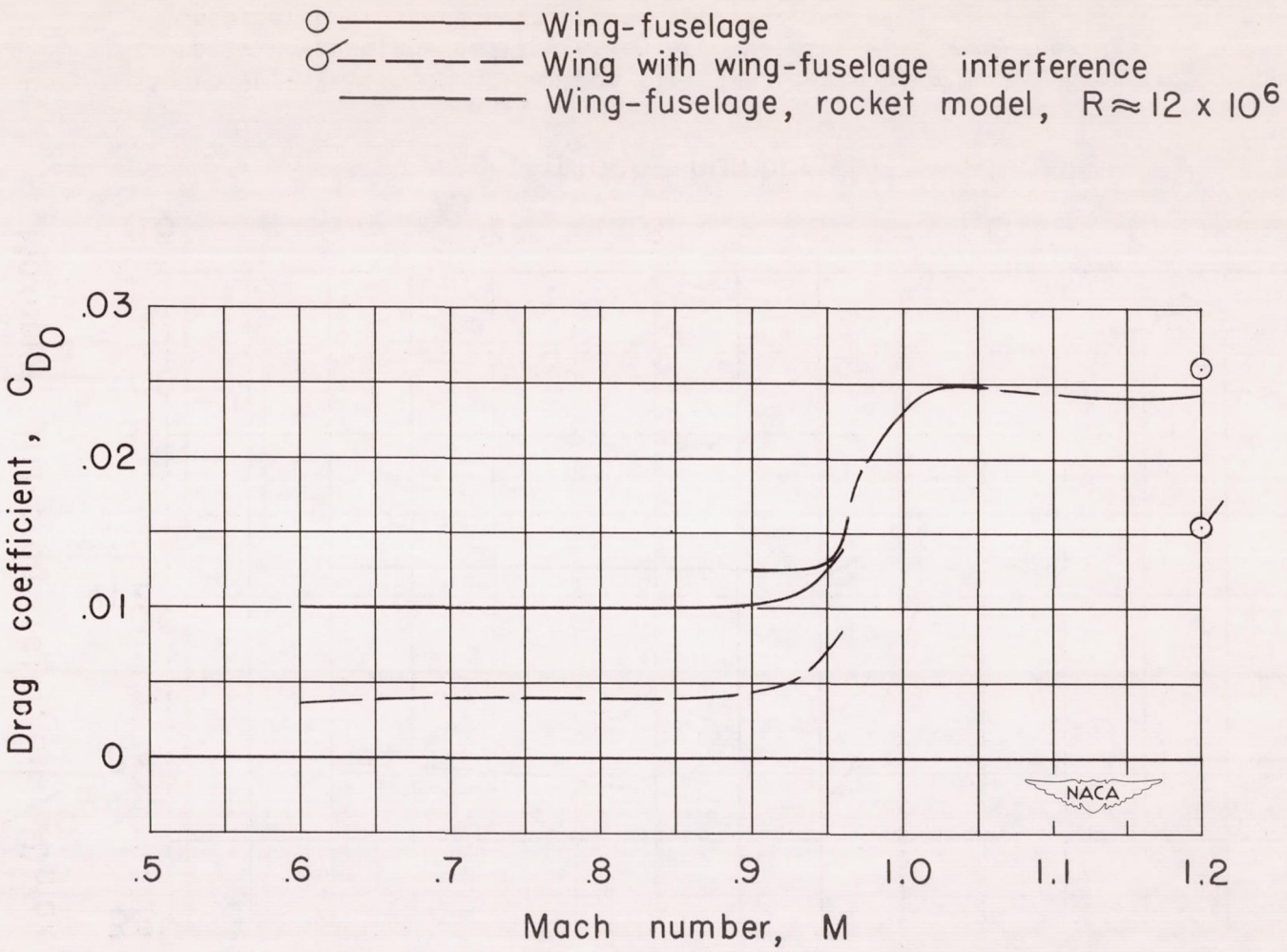


Figure 15.- Variation of drag coefficient at zero lift with Mach number for the wing-fuselage configuration and the wing with wing-fuselage interference. Tare corrections applied. Data from similar rocket model also shown.

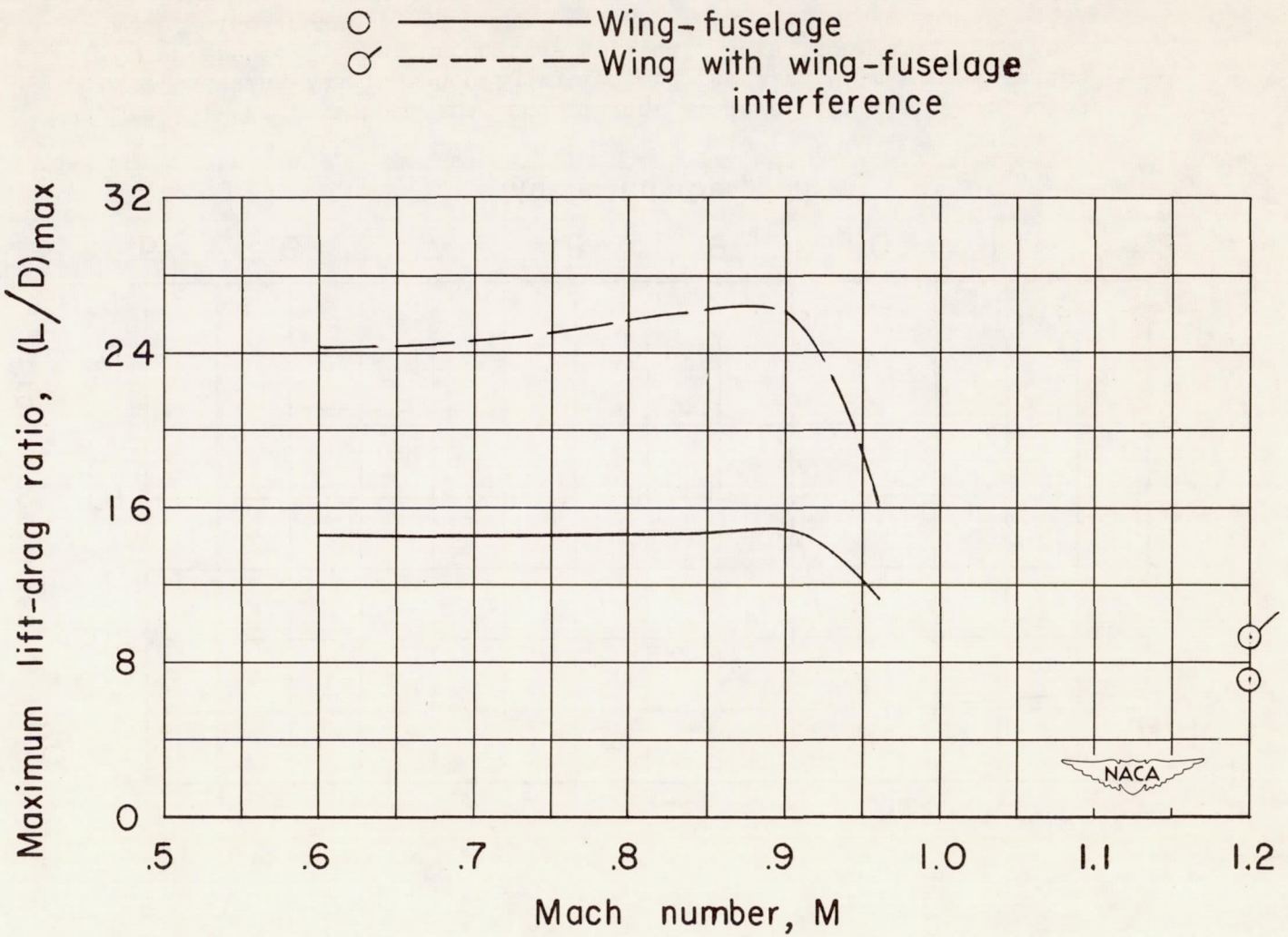


Figure 16.- Variation of maximum lift-drag ratio with Mach number for the wing-fuselage configuration and the wing with wing-fuselage interference. Tare corrections applied.

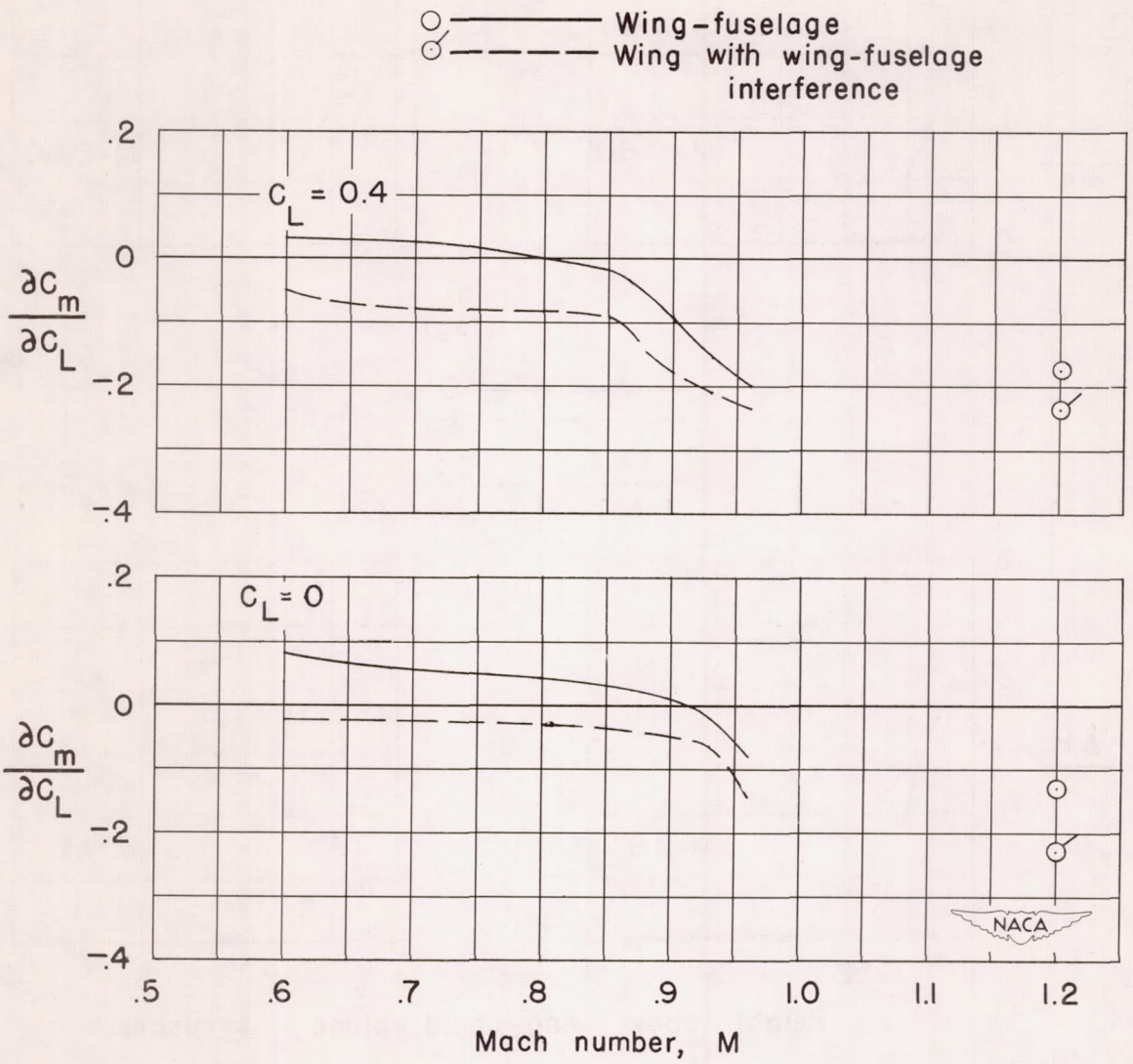
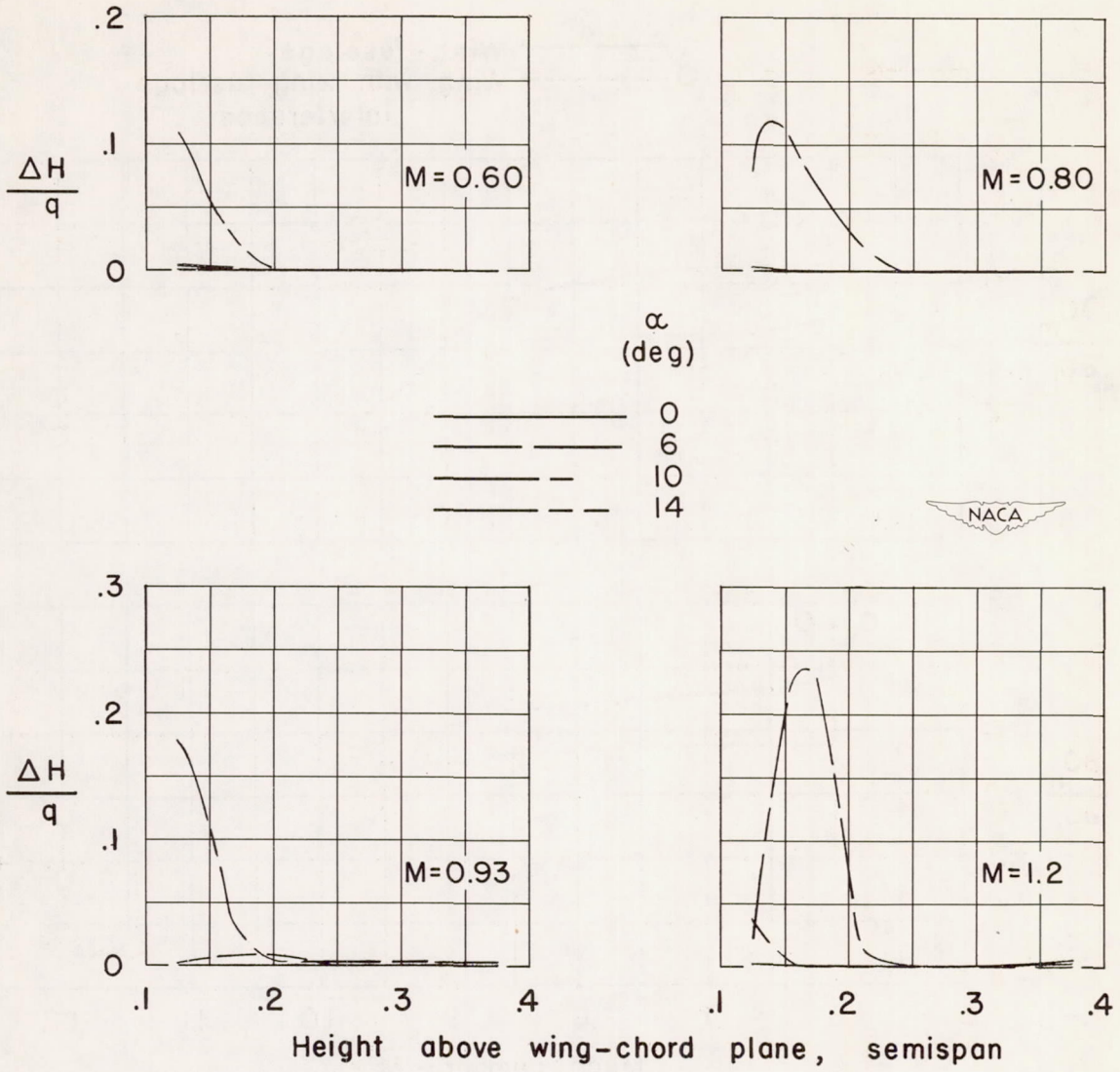
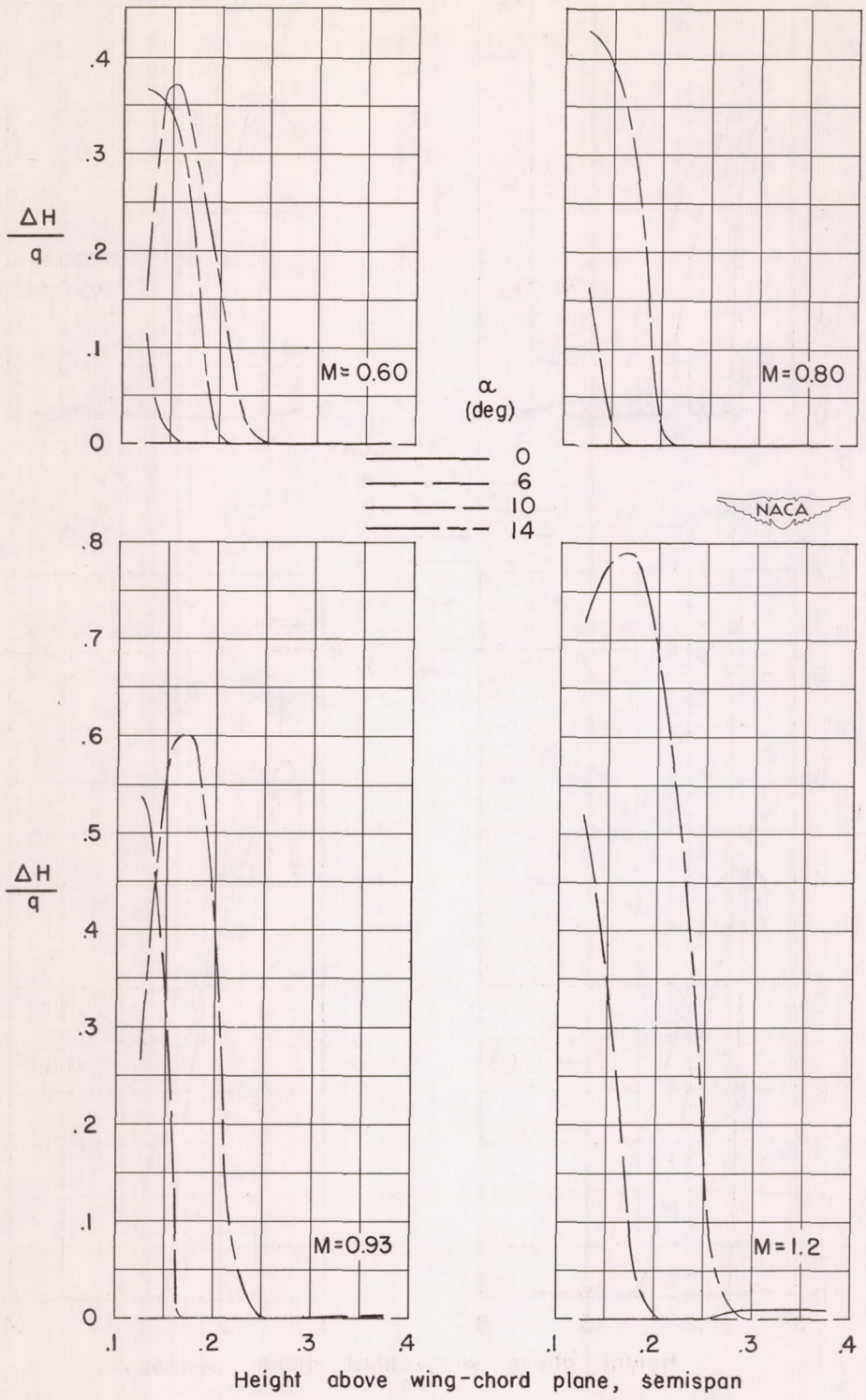


Figure 17.- Variation of the static longitudinal stability parameter with Mach number for the wing-fuselage configuration and the wing with wing-fuselage interference.



(a) Location 0.292 semispan from plane of symmetry.

Figure 18.- Wake characteristics 1.225 semispans behind the 0.25$\bar{c}$ position for the wing-fuselage configuration.



(b) Location 0.083 semispan from plane of symmetry.

Figure 18.- Concluded.

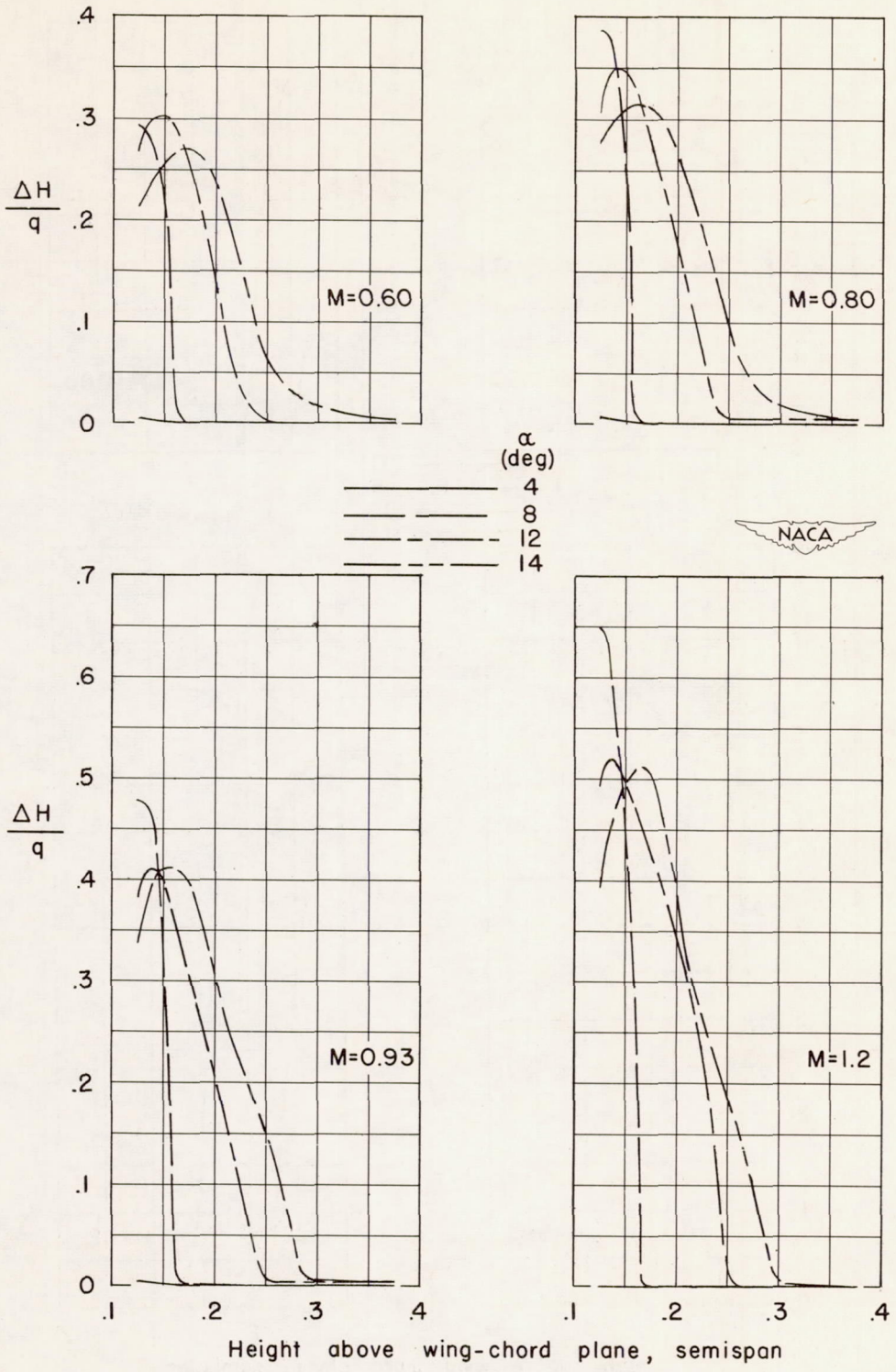
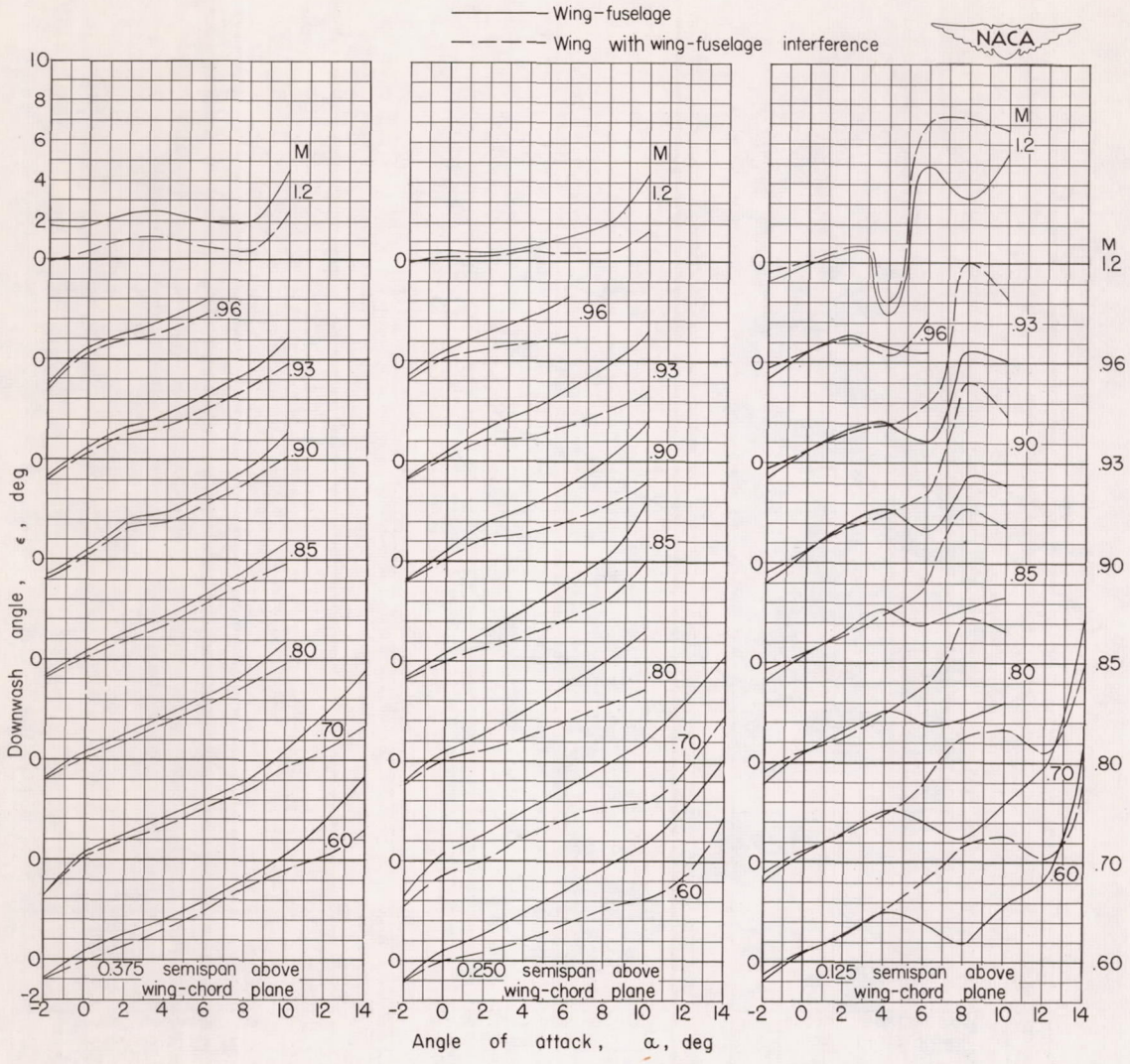
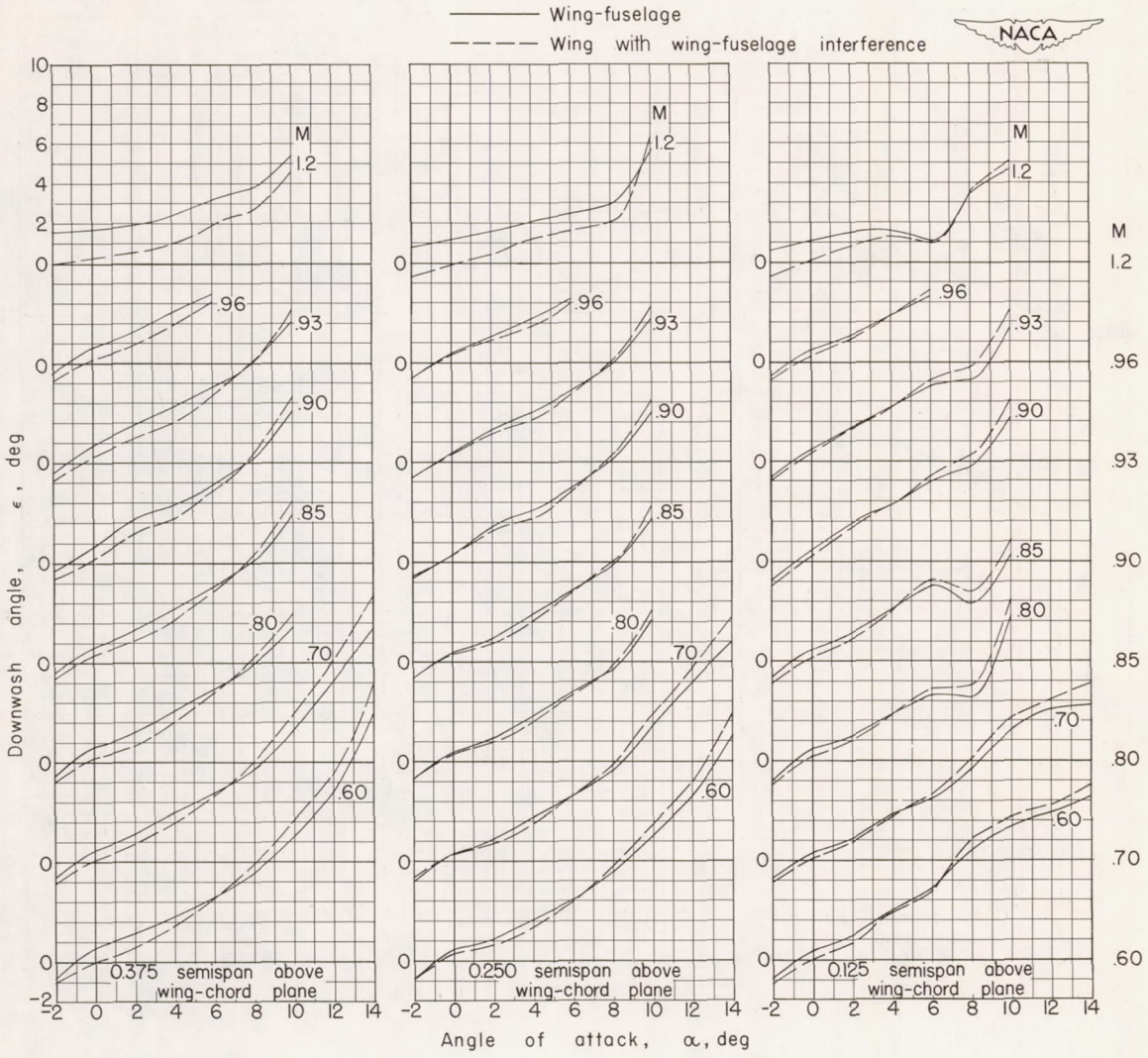


Figure 19.- Wake characteristics 1.225 semispans behind the 0.25$\bar{c}$ position and 0.083 semispan from the plane of symmetry for the fuselage configuration.



(a) Location 0.083 semispan from plane of symmetry.

Figure 20.- Variation of downwash angle 1.225 semispans behind the 0.25$\bar{c}$ position with angle of attack for the wing-fuselage configuration and the wing with wing-fuselage interference.



(b) Location 0.292 semispan from plane of symmetry.

Figure 20.- Concluded.

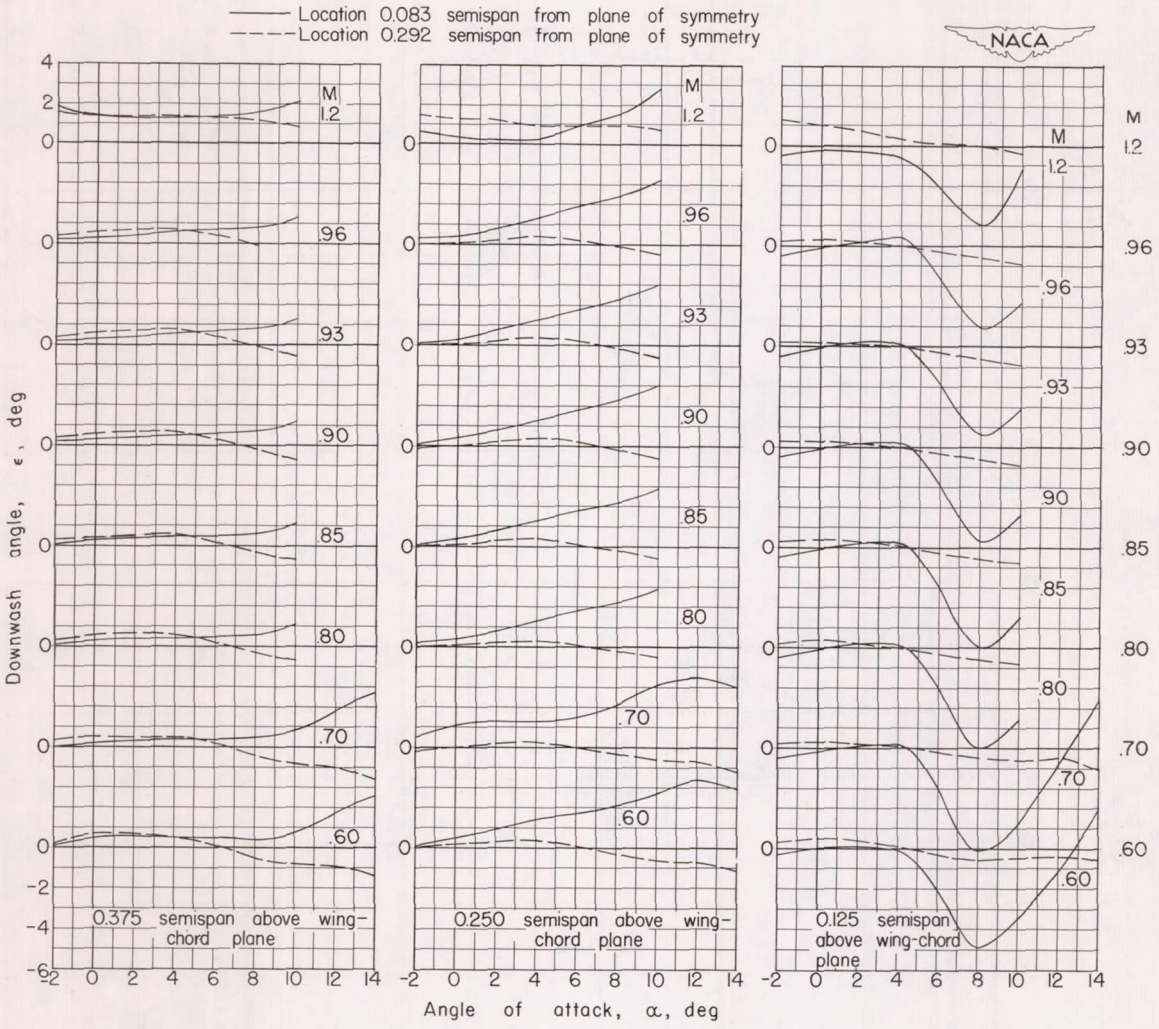


Figure 21.- Variation of downwash angle 1.225 semispans behind the $0.25\bar{c}$ position with angle of attack for the fuselage configuration.

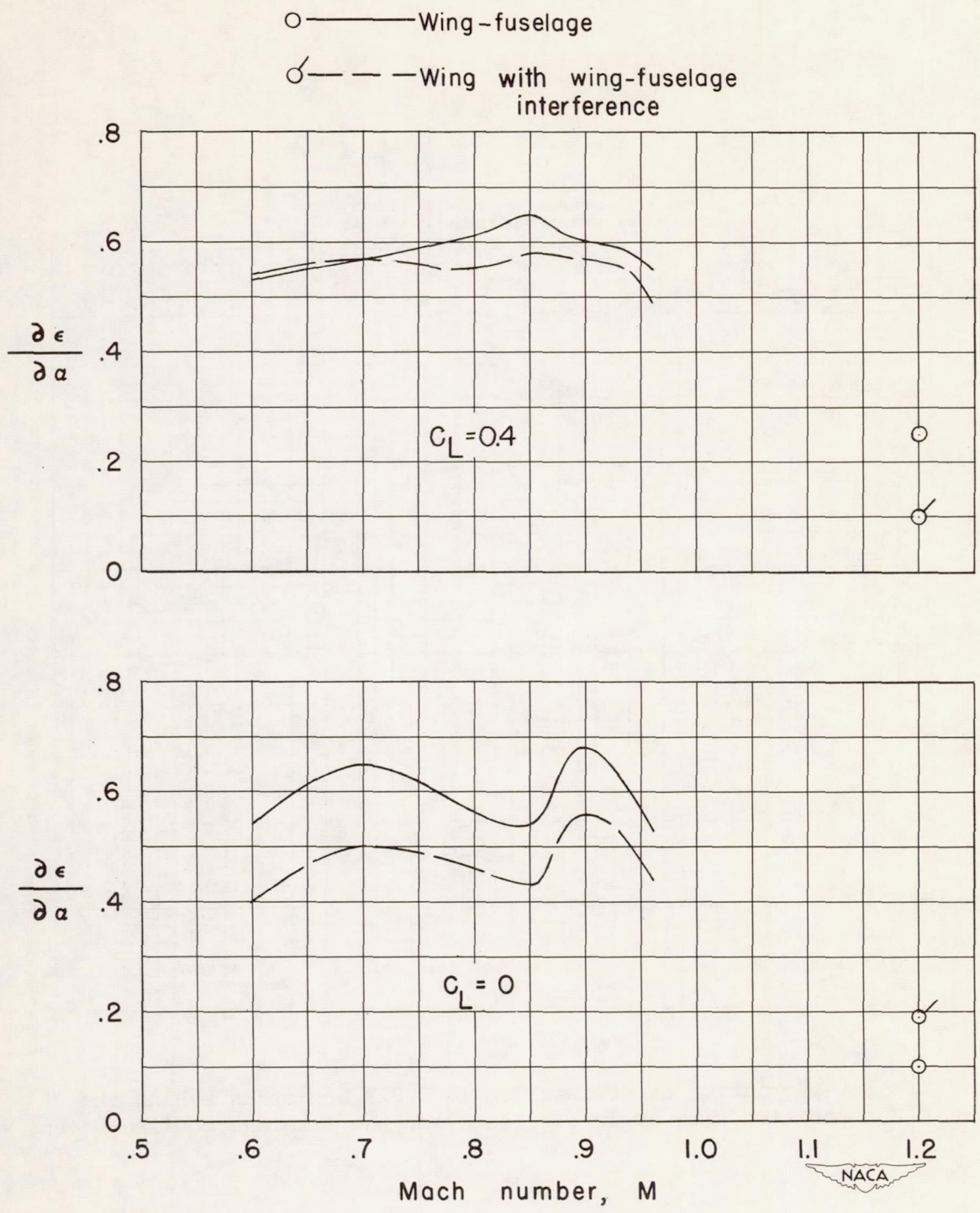


Figure 22.- Variation with Mach number of the average rate of change of downwash angle with angle of attack for a location 0.250 semispan above the wing-chord plane and 1.225 semispans behind the 0.25$\bar{c}$ position for the wing-fuselage configuration and the wing with wing-fuselage interference.

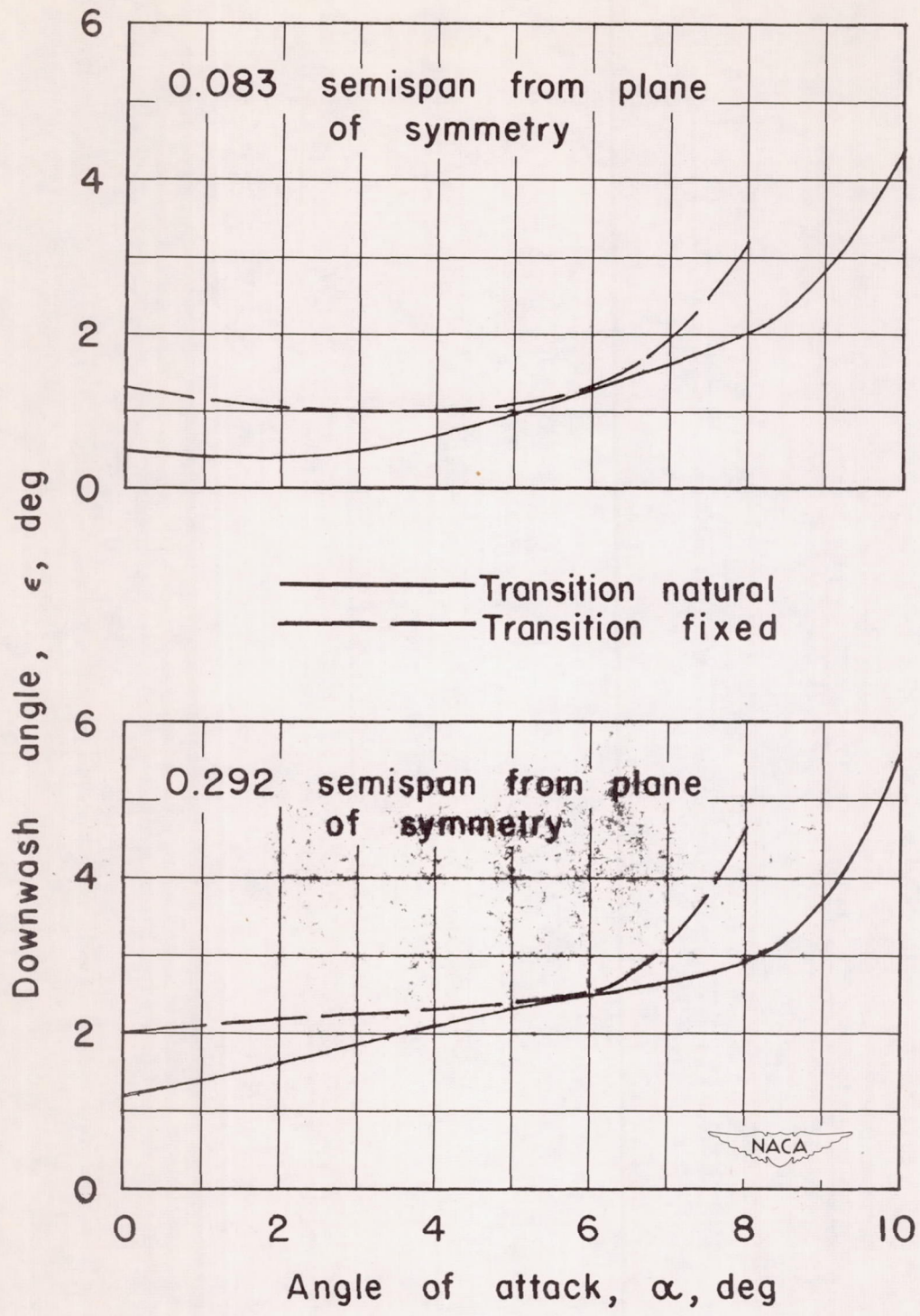


Figure 23.- Effect of fixing transition on downwash angle 1.225 semispans behind the 0.25$\bar{c}$ position and 0.250 semispan above the wing-chord plane for the wing-fuselage configuration at a Mach number of 1.2.